Journal of Materials Chemistry B

ROYAL SOCIETY OF CHEMISTRY

PAPER

View Article Online
View Journal | View Issue

Cite this: J. Mater. Chem. B, 2025, 13, 11767

Poly(*N*-acryloyl-L-phenylalanine) nanoparticles for potential treatment of inflammation in selective organs

Divya Pareek,[a] Sukanya Patra,[a] Md. Zeyaullah,[b] Gurmeet Singh,[a] Taniya Das,[a] Prakriti S. Samanta,[a] Aman S. Kudada,[a] Anjali Mourya,[a] Kirti Wasnik,[a] Rajalaxmi Pradhan,[a] Yitzhak Mastai[c] and Pradip Paik *[a]

Systemic inflammation can lead to multi-organ failure. The existing anti-inflammatory agents show adverse side effects, and the present situation demands new drugs with high therapeutic efficiency. Polymeric nanoparticles based on amino acids could be one of the best alternative solutions due to their cytocompatibility and immune responses. Herein, we synthesized polymeric nanoparticles (Phe NPs) with a size of 20–30 nm using *N*-acryloyl-L-phenylalanine methyl ester as a precursor. The biological and immune responses of Phe NPs were found to be commanding, which was proven using immune cells (RAW 264.7 macrophages). *In vitro* study revealed an easy uptake of these NPs (~98%) by the immune cells and that they can reduce inflammation by improving the immune response. *In silico* molecular docking results revealed that Phe NPs could potentially interact with immune cytokines such as IL-6, NF-κβ, TNF-α, COX2 and IL-1β. Phe NPs exhibit a similar type of binding and interaction as ibuprofen (IBF), which confirms its immune response to control inflammation. The anti-inflammatory response of Phe NPs was established through an *in vitro* inflammation model developed using LPS-stimulated RAW 264.7 macrophages. Furthermore, an LPS-induced *in vivo* rat model was developed, which revealed that Phe NPs are useful for the treatment of systemic inflammation. Blood-based biochemical parameters such as C-reactive protein, lactate and procalcitonin levels were determined, and the anti-inflammatory responses of Phe NPs were confirmed through RT-PCR analysis by measuring the levels of inflammatory markers such as TNF-α, IL-6 and VEGF. Finally, an *in vivo* systemic inflammation rat model was used to examine the systemic organs (brain, liver, kidneys, spleen, lungs and heart) before and after treatment with Phe NPs to prove their anti-inflammatory responses. H&E histological analysis of different organs further revealed that even at a low dose of 100 μg kg^{-1}, Phe NPs are immune-responsive/protective and anti-inflammatory in nature.

Received 15th April 2025,
Accepted 11th August 2025

DOI: 10.1039/d5tb00886g

rsc.li/materials-b

1. Introduction

Systemic inflammation may cause multi-organ failure and increase the mortality rate if suitable treatments are not provided.[1] It contributes to cardiovascular diseases, various types of cancers, diabetes mellitus, chronic kidney diseases, non-alcoholic fatty liver disease, and autoimmune and neurodegenerative disorders.[2]

Identifying the exact cause of systemic inflammation is difficult, as it may be caused by external (biological or chemical agents) or internal (genetic mutations/variations) factors. Patients with this condition often have high levels of inflammatory markers.[3] Systemic inflammation presents several challenges related to its diagnosis, impact on overall health and therapeutic interventions. Current anti-inflammatory medications such as corticosteroids for more serious inflammation and NSAIDs (non-steroidal anti-inflammatory drugs) such as ibuprofen (IBF), naproxen and aspirin for less severe cases have disadvantages such as non target specific action, adverse reactions and requirement for high dosages.[4] It may additionally lead to stomach ulcers, high blood pressure and compromised immune systems when utilized for an extended period of time. Other advanced therapies such as gene therapy,[5] immune therapy[6] and CAR-T cell therapy[7] create a financial burden, physical pain and organ dysfunction, and at the same time, alternative biological treatments are intended to provide relief and improved quality of life for patients.[8]

[a] School of Biomedical Engineering, Indian Institute of Technology, Banaras Hindu University, Varanasi, Uttar Pradesh 221 005, India. E-mail: paik.bme@iitbhu.ac.in, pradip.paik@gmail.com
[b] Department of Zoology, Banaras Hindu University (BHU), Varanasi, Uttar Pradesh 221 005, India
[c] Department of Chemistry, Bar-Ilan University, Ramat-Gan 5290 002, Israel

Recently, various biomaterials have been developed to modulate inflammation in various conditions to address reactive oxygen species (ROS),[9] reactive nitrogen species (RNS)[10] and cell-free DNA in the early stages of inflammation.[11] Few cell-inspired polymeric nanoparticles (*e.g.* poly(lactide-*co*-glycolide), phosphatidylserine (PS), polyethene glycol (PEG))[12] and inorganic nanoparticles (*e.g.*, Au, Fe_3O_4, SiO_2, and Ag-MOF)[13] are also used as therapeutics that inhibit inflammation by releasing anti-inflammatory cytokines, sequestering proinflammatory cytokines and promoting phenotype switching of macrophages. Nanoparticle-based approaches to prevent systemic inflammation have gained potential, notably for modifying the immune response and mitigating the severe effects of cytokine storms.[14] Further, NPs can control the inflammation by releasing anti-inflammatory components or improving the bioavailability of drugs at the inflammatory sides. Natural biomaterials such as hyaluronic acid, chitosan and collagen have intrinsic anti-inflammatory properties.[15] Synthetic biomaterials, *e.g.*, PLGA and PLA, are also reported for their anti-inflammatory activities. PLA can reduce the TLR activation and subsequent pro-inflammatory cytokine release.[16] In this line, amino acid-based polymeric nanoparticles (PNPs) can be used for treating systemic inflammation due to their lower toxicity and higher bioavailability,[17] and they can be engineered to modulate immune responses.[12,17] However, existing therapeutics and approaches of treatment are not able to meet the therapeutic demand.

In these circumstances, we plan to use amino acid-based polymeric NPs without any conventional drug for monitoring the systemic inflammation. This work is taken into consideration since amino acids are shown to be effective supplements during inflammatory conditions.[18] It is also reported that essential amino acids (EAAs) were administered to elderly patients in rehabilitation after acute diseases to reduce the inflammatory state.[18] Our recent report has shown the impact of controlling inflammation due to rheumatoid arthritis (RA) diseases using poly(*N*-acryloyl glycine) nanoparticles.[19] However, none of the work was reported on mitigating the systemic inflammation using amino acid-based polymeric nanoparticles. Using the precursor material phenylalanine (Phe) and suppressing the production of TNF-α and IL-1β in inflammatory (M1) macrophages, the current research could potentially be one of the treatment options for the therapy integrating all the beneficial aspects of the earlier treatments.

L-Phenylalanine is shown to serve as a selective inhibitor of epithelial alkaline phosphatase.[20] While phenylalanine is not directly classified as an anti-inflammatory medication, its derivatives have considerable anti-inflammatory capabilities, indicating that the structural changes can improve the therapeutic effects,[21] as the L-enantiomer of Phe retains its natural configuration, which can facilitate more favourable interactions with chiral biological systems such as enzymes, cell membranes and receptors. This can enhance the biocompatibility and cellular uptake and potentially contribute to the observed anti-inflammatory effects.[22]

Our hypothesis is that by synthesizing specifically designed amino acid phenylalanine-based nanoparticles, we could combine two specific systems with more benefits such as the amino acid acting as a base material and its nano-size showing a better inflammatory response. With this aim, this work is focused on the synthesis of poly(*N*-acryloyl-L-phenylalanine methyl ester) nanoparticles (Phe NPs). *In vitro* studies on various cell lines (*e.g.*, L929, PC-12, HEK293 and RAW 264.7 macrophage immune cells) were conducted to determine the biocompatibility of Phe NPs at different concentrations, and the anti-inflammatory behaviour of the Phe NPs was confirmed through RT-PCR.

In silico docking analysis on target proteins that are responsible for inflammation using Phe NPs was performed to find out its binding affinity/energy and the results were compared with commercially available anti-inflammatory drugs, *e.g.*, Ibuprofen (IBF). An *in ovo* angiogenesis analysis was performed, and the dose-dependent anti-angiogenic nature of Phe NPs was studied to find out their anti-inflammatory potential. The hemocompatible tests with different concentrations of Phe NPs were conducted to decide the best doses for treatment. Their potential was also checked in an *in vivo* systemic inflammation model using Wistar rats. The effect of treatment on the LPS-induced rats was checked after a predefined treatment period. The levels of biochemical markers (*e.g.*, C-reactive protein (CRP), lactate and procalcitonin) were measured. After 24 h of treatment, the rats were euthanized, and their selective systemic organs (*e.g.*, brain, lungs, liver, kidneys, heart and spleen) were harvested for morphological and histopathological analyses, which provided insightful results for the Phe NP response on each body organ after inflammation conditions. The effective suppression of systemic inflammation by Phe NPs was established by estimating the organ weight and inflammatory biochemical and proinflammatory cytokine levels of TNF-α, IL-6 and VEGF. Finally, the results demonstrate the potential of Phe NPs for the treatment of inflammatory diseases.

2. Results and discussion

2.1. Synthesis of Phe monomers and polymeric Phe NPs

The phenylalanine-based nanoparticles were synthesized in two significant steps. A monomer was initially prepared and then polymeric nanoparticles were synthesized. L-Phenylalanine methyl ester hydrochloride was initially used to synthesize monomers by following the method mentioned in our earlier work.[23,24] A modification was done by increasing the sonication time to achieve NPs with a smaller size. The monomer was prepared followed by the Shortens-Baumann reaction. In the 1st step, *N*-acryloyl-L-phenylalanine methyl ester was dissolved in oil-phase toluene to form monomer droplets. Hexadecane was used as a co-stabilizer. The AIBN was used as a free radical initiator for polymerization. DVB was used as a cross-linking agent between two monomers, which provides mechanical stability to the polymeric particles. SDS was used as a surfactant to avoid aggregation. Further, by washing with a water–ethanol mixture, excess SDS was removed. A detailed synthesis method is presented in the methods section.[25]

The formation of monomers and polymers and their chemical functionality were confirmed through ^{1}H-NMR 500 MHz, $CDCl_3$), ^{13}C-NMR (125 MHz, $CDCl_3$) and ^{13}CP-MAS (^{13}CP NMR, 600 MHz) experiments (Fig. S1–S3). The characteristic FTIR bands for monomers appeared at 3428 cm^{-1} (for NH_2/–OH), 2932 cm^{-1} (for $–CH_2–/–CH_3$), 1748 cm^{-1} (for –C═O), 1682 cm^{-1} (for –NH–) and 1516 cm^{-1} (for –OH). Similarly, for polymers (Phe NPs), the characteristic bands for functional groups appeared at 3334–3028 cm^{-1} (for NH_2/–OH), 2952 cm^{-1} (for $–CH_2–/–CH_3$), 1743 cm^{-1} (for –C═O), 1660 cm^{-1} (for –NH–) and 1540 cm^{-1} (for –OH) (Fig. 1(a)). To check the size and morphology of Phe NPs, TEM images were acquired using a carbon-coated Cu-grid (200 mesh). For sample preparation, a pinch of Phe NPs was taken and suspended in isopropanol followed by sonication for dispersion of Phe NPs. The images were acquired at different magnifications (Fig. 1(b and c)). The TEM results revealed that Phe NPs are 19 to 30 nm in diameter (Fig. 1(b and c)). AFM analysis was also performed, and the particle size results obtained (Fig. 1(d and e))

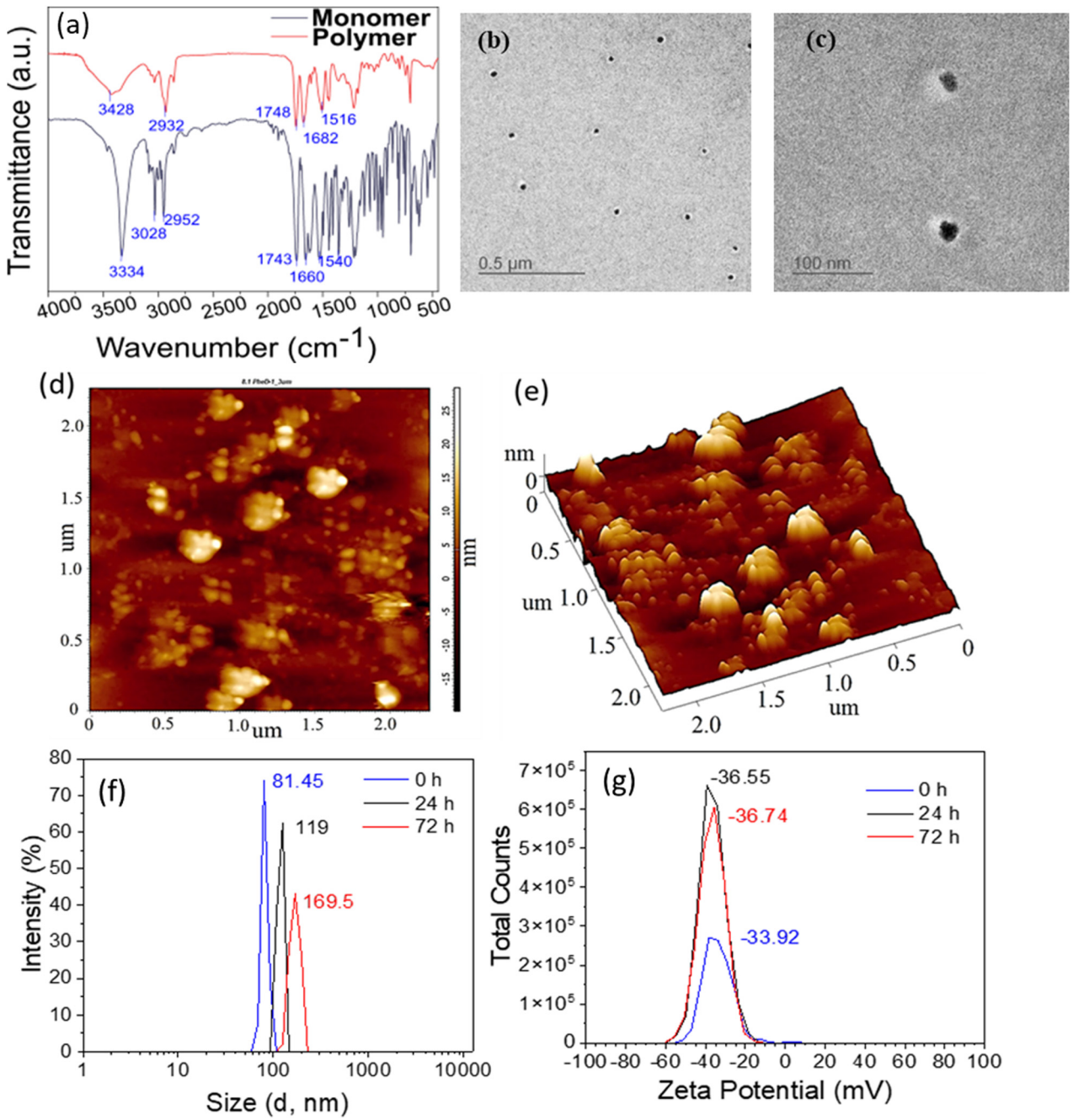

Fig. 1 Physical Characterization of Phe monomers and Phe NPs. (a) FTIR spectra of Phe monomers and Phe NPs, (b) TEM micrograph of Phe NPs, scale: 0.5 μm. (c) TEM image of Phe NPs, scale: 200 nm. (d) AFM 2D surface topography image of Phe NPs obtained using an AFM. (e) AFM 3D image of Phe NPs. (f) Size distribution of Phe NPs measured at physiological pH ∼ 7.4 at 0, 24 and 72 h by DLS at 25 °C, and (g) profile for the zeta potential of Phe NPs measured at 0, 24 and 72 h at 25 °C.

are comparable to the TEM results (Fig. 1(b and c)). AFM topography 2D (Fig. 1(d)) and 3D (Fig. 1(e)) images confirmed that Phe NPs are spherical in size. Further, the size and the colloidal stability of Phe NPs were measured at physiological pH (7.4) by DLS and zeta potential measurements, respectively (Fig. 1(f and g)) at 25 °C with different time periods, namely, 0 h, 24 h and 72 h.

The average hydrodynamic diameter of the nanoparticles was calculated to be 119 nm (in PBS, at pH 7.4). It is interesting to note that over the time periods of 0, 24 and 72 h and from DLS, the hydrodynamic size was obtained to be 81.45 nm, 119.8 and 169.5, respectively, with time due to the swelling of the particles in aqueous media. The zeta potential (ζ) also changed (minor) with time, namely −33.92 mV, −36.55 mV and −36.74 mV, respectively, indicating that the Phe NPs are stable as a colloidal suspension at physiological pH (7.4).

2.2. *In vitro* biocompatibility of Phe NPs

The polymeric nanoparticles must be biocompatible to justify their usefulness as therapeutics. As mentioned earlier, the MTT assay was performed to check the biocompatibility of Phe NPs on L929, HEK 293, PC12 and RAW 264.7 macrophages.

The cell viability was checked at different concentrations (1, 5, 10, 25, 50, 100, 250, 500 and 1000 μg mL^{-1}) of Phe NPs (Fig. 2). The cell viability at a very low concentration of Phe NPs (1 μg mL^{-1}) was found to be 133.31 ± 6.72% against L929 cells, indicating that it is proliferative in nature (Fig. 2(a)). As the concentration of Phe NPs increases to 500 μg mL^{-1}, the cell viability was determined to be 101 ± 5%, and at 1 mg mL^{-1}, the viability was found to be 76.35 ± 12.76% (Fig. 2(a)). Thus, Phe NPs are compatible with L929 cells. Then, the viability was checked on the HEK-293 cell line with different concentrations of Phe NPs (1, 5, 10, 25, 50, 100, 250, 500 and 1000 μg mL^{-1}) (Fig. 2(b)). Phe NPs are proliferative in nature (145.82 ± 9.2%) at low concentrations (1 μg mL^{-1}). At 500 mL^{-1}, the cell viability was found to be 72.83 ± 2.66%. Further, to check the effect of Phe NPs on the neuronal cell line, PC-12 cells were selected, which comprise a neuroblastoma cell line. In PC-12 cells, as the concentration changes from 10, 20, 40, 80, 100, 125, 150, 200 to 250 μg mL^{-1}, the cell viability was found to be 115.90 ± 1.80, 110.52 ± 5.49, 106.08 ± 12.54%, 98.01 ± 17.80%, 88.36 ± 7.70%, 83.21 ± 16.02%, 81.63 ± 5.80%, 72.74 ± 5.81% and 68.18 ± 12.54%, respectively (Fig. 2(c)). The most interesting part of this study is the response of

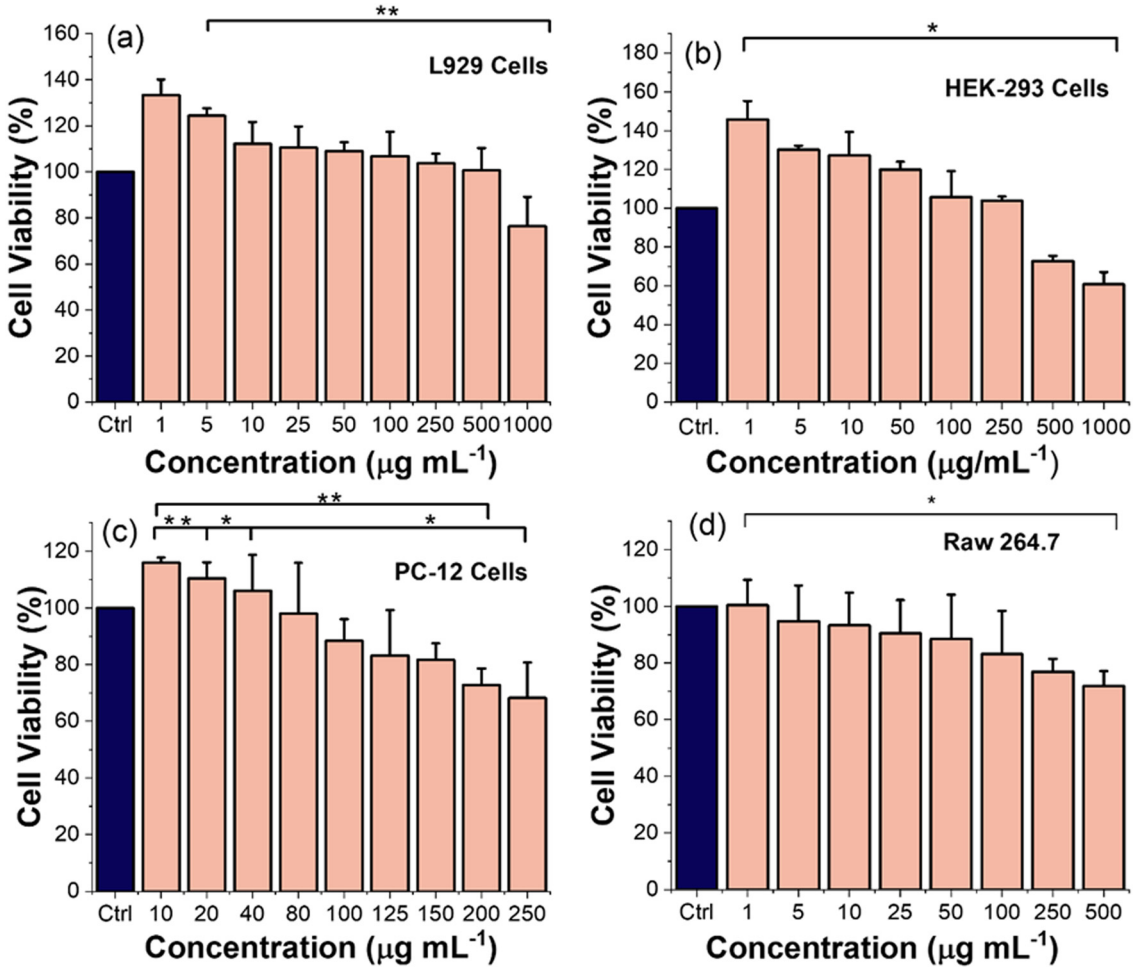

Fig. 2 Cell viability of Phe NPs. Studied with Phe NPs at different concentrations, such as 1, 5, 10, 25, 50, 100, 250, 500 and 1000 μg mL^{-1}, through an MTT assay on (a) L929, (b) HEK-293, (c) PC-12 and (d) RAW 264.7 macrophages. Experiments were performed at 37 °C, 5% CO_2, using 1 × 10^5 cells per well. Viability was checked after 24 h of incubation with Phe NPs. *$p < 0.05$, **$p < 0.01$.

the immunological cell line (RAW 264.7 macrophages) against Phe NPs.

In RAW 264.7 macrophages, at different concentrations of Phe NPs (1, 5, 10, 25, 50, 100, 250 and 500 μg mL^{-1}), the viability (%) was determined to be 100.42 ± 8.95, 94.78 ± 12.64, 93.26 ± 11.55, 90.46 ± 11.75, 88.43 ± 15.70, 83.10 ± 15.27, 76.93 ± 4.55 and 71.80 ± 5.33, respectively (Fig. 2(d)). Thus, Phe NPs exhibit good viability with different cell lines, as shown in Fig. 2(a–d).

2.3. *In vitro* cellular uptake of Phe NPs by immune cells (RAW 264.7 macrophages)

Cellular uptake and internalization of nanoparticles/polymers are significant phenomena. Due to the cellular internalization, various biological changes can occur.[26] The dynamic movement of polymeric NPs towards different organoids is strongly controlled by the cellular components, thereby controlling the therapeutic efficiency. Therefore, the cellular uptake of Phe NPs was assessed by confocal microscopy and fluorescence-activated cell sorting. For confocal microscopy, Phe NPs were stained with Nile red for 24 h and then the stained NPs were incubated with RAW 264.7 macrophages for 24 h at a safe concentration of 100 μg mL^{-1}. Following this incubation, the cells were fixed and stained with DAPI to visualize the nuclei. Confocal microscopic images were acquired with Nile red-labelled Phe NPs (Fig. 3(a–f)). The DAPI-stained nuclei were observed using the blue fluorescence channel (λ_{max} = 405 nm) (Fig. 3a). In contrast, the fluorescence light emitted from Phe NPs was detected in the red channel (λ_{max} = 546 nm) (Fig. 3b).

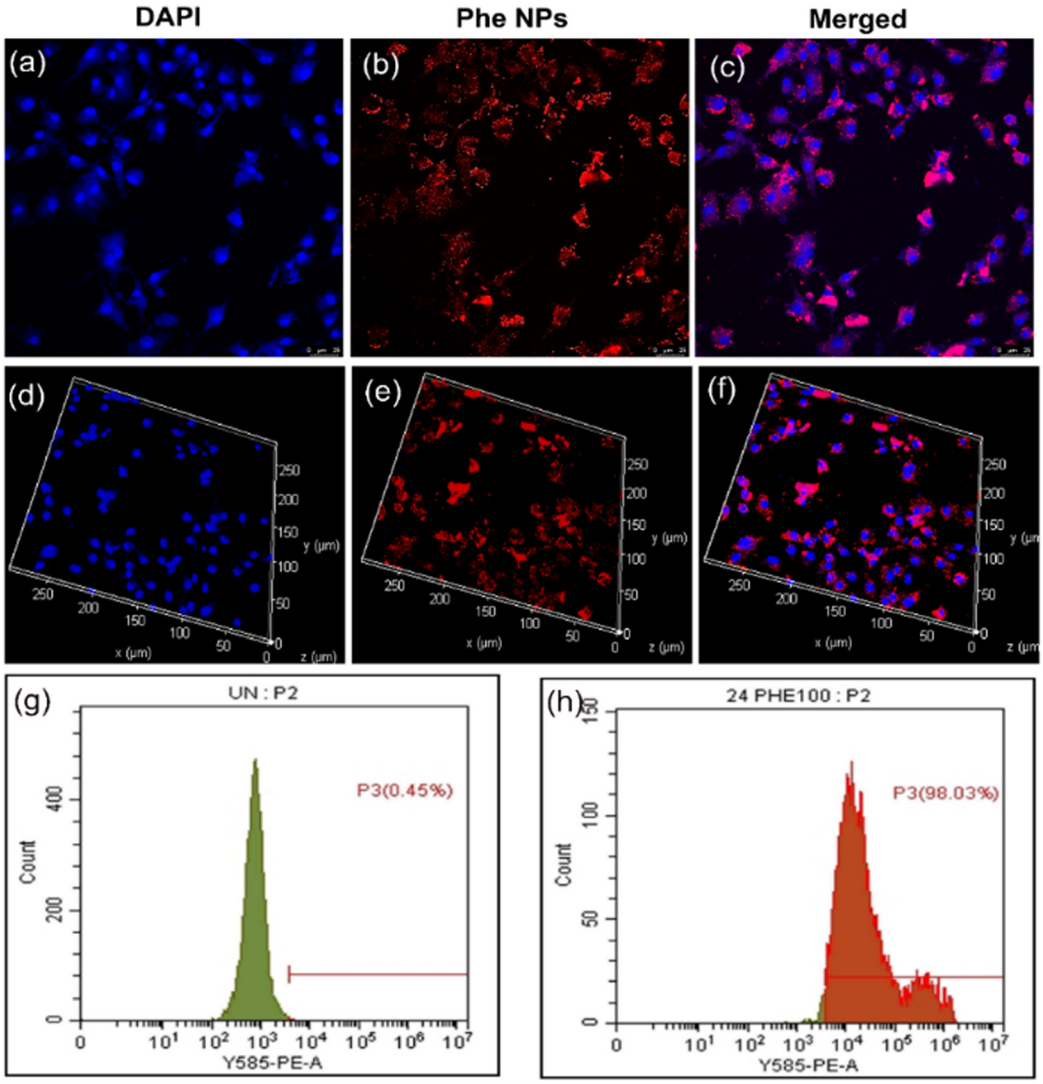

Fig. 3 Cellular uptake of Phe NPs in RAW 264.7 macrophages. (a)–(f) Confocal microscopy images: (a) 2D representation of DAPI-stained nuclei, observed using the blue fluorescence channel (λ_{max} = 405 nm); (b) 2D images of cells incubated with the Nile red-labelled Phe NPs observed using the red fluorescence channel (λ_{max} = 546 nm); (c) 2D representation of the merged images of (a) and (b), indicating that Phe NPs were successfully internalized into the cytoplasm and nuclei of the RAW 264.7 macrophages within 24 h; (d)–(f) cellular internalization 3D representation; (g) and (h) Cellular internalization of Phe NPs was assessed through FACS using the RAW 264.7 macrophages ((g) is for the control unstained cell sample and (h) shows the FACS results for using the RAW 264.7 macrophages incubated with Rhodamine-tagged Phe NPs (100 μg mL^{-1}), indicating 98.03% internalization of Phe NPs).

Fig. 3(c) shows the 2D representation of merged images of Fig. 3(a) and (b), which indicate that the Phe NPs were successfully internalized into the cytoplasm and nuclei of the RAW 264.7 macrophages within 24 h of incubation. There are defined mechanisms of internalization of Phe NPs such as endocytosis. However, it can also be through the mixed mechanisms (clathrin-mediated, caveolae-mediated endocytosis or macropinocytosis).[26]

Further, the cellular internalization of Phe NPs is also confirmed through the FACS. RAW 264.7 macrophages (1×10^4) were incubated with Rhodamine-tagged Phe NPs (100 μg mL^{-1}), and they were harvested for 24 h and washed to remove the unbound nanoparticles. The live single-cell population was gated in a plot of FSC *versus* SSC after excluding cell debris and doublets. Then a histogram from the Y585-PE-A channel for the single-cell population was obtained (Fig. 3(g and h)) using the FlowJo software (version X, FlowJo LLC). It is revealed that 98.03% Phe NPs are internalized (Fig. 3g and h) in macrophages. Further, the median fluorescence intensity (MFI) is observed to be significantly higher in extent for treated cells compared to the control samples, confirming that the Phe NPs were effectively internalized into the cells. Further, it can be predicted that the uptake of Phe NPs by immune cells could influence different cellular signalling pathways, potentially leading to the reduction of inflammation by improving the immune responses, which is not the main focus of this study.[27,28]

2.4. *In silico* molecular docking study: interactions between Phe and inflammation-targeted protein receptors

Molecular docking is important for identifying the target protein and ligand orientation for a stable complex after binding. To identify the desirable domains most likely to bind to proteins of interest, docking was performed to screen enormous databases of possible medicinal compounds *in silico* within a short period of time.[29] The binding energy of commercially available IBF and our Phe NPs was compared to check their significant effects on inflamed markers such as IL-6, IL1β, NF-κβ, TNF-α and COX-2 (Fig. S4).

IL-6 (pdb id 1ALU) plays a significant role especially for the systemic inflammation.[30] For an *in silico* study, it is essential to check the binding energy of IL-6 with *N*-acryloyl-L-phenylalanine, and the results have been compared with IBF. As a cytokine, IL-6 can exacerbate acute inflammation, which aids in developing chronic inflammation and assists in autoimmune events. In response to infections and tissue damage, IL-6 are temporarily produced. It also supports host defence by inducing immunological, hematopoiesis and acute phase responses.[31] Thus, the binding energy for both IL-6 and IBF was calculated to be −5.90 kcal mol^{-1}, and the residues involved in H-bonding are Arg182, Leu178, Gln175, Arg30, Leu33 and Arg179 grooves, whereas the binding energy for Phe NPs was determined to be −6.17 kcal mol^{-1} and the residues associated are Leu33, Gln175, Arg179, Arg182 and Leu178. These results further reveal that the Phe is binding more strongly with IL-6 than IBF, where almost all the residues are involved in forming H-bonding (Fig. 4(a and f) and Table S1).

NF-κβ (pdb id 1VKX) is a primary transcription factor for inflammation.[32] NF-κB induces the expression of pro-inflammatory cytokines such as TNF-α, IL-1 and IL-6, and chemokines present in monocytes and macrophages.[33] For IBF, the binding energy with NF-κβ (pdb id 1VKX) was calculated to be 5.59 kcal mol^{-1} and the available residues for H-bonding are Lys414, Ala435, Leu437, Cys421, His415, Phe434, Val423 and Gly433. However, for Phe, the binding energy was determined to be −5.13 kcal mol^{-1}, and the residues involved in H-bonding are His415, Lys414, Ala 435, Gly433 and Phe434 (Fig. 4(b and g)). The detailed results are presented in Table S1.

TNF-α (2AZ5) is a chemical messenger or cytokine primarily produced by activated macrophages, which induces chronic inflammatory disorders.[34] The binding energy for the 2AZ5 protein receptor with IBF was calculated to be −5.88 kcal mol^{-1} and H-bonding residues are formed with the residues Ile155, Leu157, Lys11, Asp10, Asn39, Pro12, Val13 and Ala156, whereas for the Phe, the binding energy was calculated to be −3.85 kcal mol^{-1} and the grooves are Asp10, Lys11, Val13 and Ile155, as shown in Fig. 4(c and h). The detailed results are shown in Table S1.

For cyclooxygenase-2 (COX2) (pdb id 3LN1), the AutoDock results reveal that COX-2 with IBF is showing a binding energy of −6.01 kcal mol^{-1} and H-bonding residues are lying at Ile503, Ala502, Phe504, Arg499, Leu338, Val509, Ala513, Ser339, His75 and Gln178, whereas, for Phe, the binding energy was calculated to be −5.62 kcal mol^{-1} and the residues involved are Ala502, Phe504, Arg499, His75, Leu338, Ser339, Gly512, Val509 and Val335. COX-2 is an enzyme that plays a crucial role in inflammation by producing prostaglandins.[35] Further, the Phe show the formation of a similar type of binding as IBF, which is a strong evidence towards its immune modulating property (shown in Fig. 4(d and i) and Table S1).

Finally, for IL-1β (pdb id 5I1B), docking was performed as it mediates systemic inflammation by producing proinflammatory cytokines. IL-1β can activate various immune cells, including macrophages, neutrophils and T-cells, by enhancing the inflammatory cascade.[36] The binding energy of IBF with IL-1β was calculated to be −5.95 kcal mol^{-1}, and the grooves that are involved in H-bonding are Val132, Glu25, Leu80, Phe133, Leu134, Lys77, Thr79 and Tyr24. The Phe NPs show a similar extent of binding energy, *i.e.*, −5.95 kcal mol^{-1}, and the grooves are found almost identical with Lys65, Leu62, Val40, Val19, Met20, and Gln38. The details of the 2D and 3D interactions are shown in Fig. 4(e and j) and Table S1.

2.5. *In vitro* immune response of Phe NPs

2.5.1. Estimation of *in vitro* NF-κβ levels for regulating inflammatory responses. The regulation of responses to inflammation is a well-known role of NF-κβ. The canonical and noncanonical (or alternative) are the two fundamental pathways of signalling that activate NF-κβ. While having different signalling mechanisms, both the pathways show significance for controlling inflammatory and immunological responses.

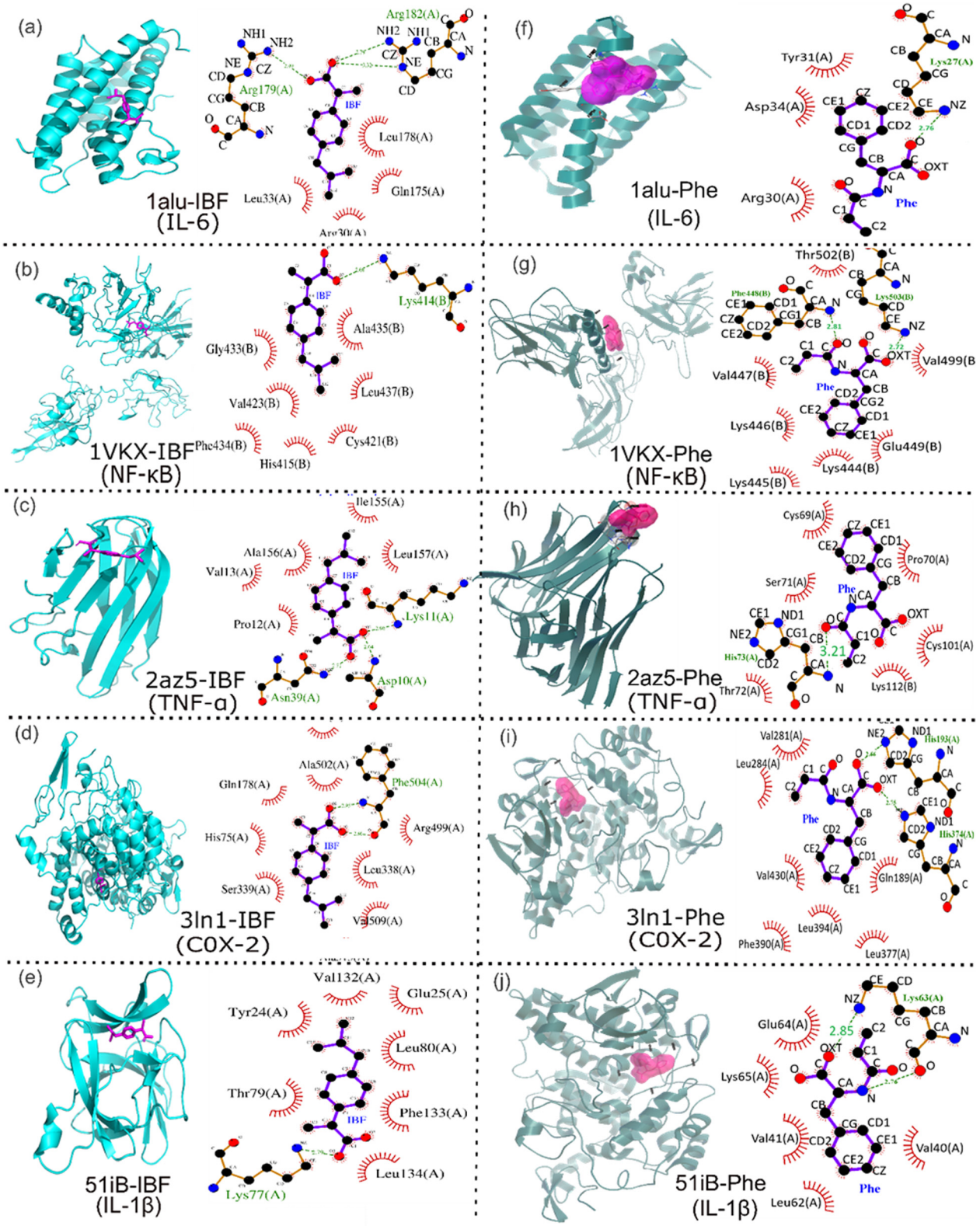

Fig. 4 AutoDock results for Phe and IBF with inflammation-specific markers. IBF interacted with (a) IL-6, (b) NF-κβ, (c)TNF-α, (d) COX-2, and (e) IL-1β. (f), (g), (h), (i) and (j) Interactions of Phe with IL-6, NF-κβ, TNF-α, COX-2 and IL-1β, respectively.

The NF-κβ signal transduction pathway can be initiated by TNFα, IL-1 and IL-18.[37] Its activation contributes to the pathogenic processes of various inflammatory diseases such as autoimmune diseases (psoriasis, ankylosing spondylosis, Crohn's disease,

ulcerative colitis, *etc.*), cardiovascular diseases (high blood pressure, heart diseases, *etc.*) or lung diseases (asthma, chronic obstructive pulmonary diseases (COPD), *etc.*).[37] The reporter colourimetry assay Quanti Blue has been employed to detect the secreted alkaline phosphatase (SEAP) level. By knowing the SEAP level, NF-κβ expression can be correlated.[38] The SEAP levels were calculated by measuring the OD value at λ_{max} = 630 nm (Fig. 5(a)). Under the control condition (with only RAW 264.7 macrophages), the SEAP level was calculated to be 1.18 ± 0.31. To check the efficiency of reducing the inflammation due to the NF-κβ level by Phe NPs, RAW 264.7 macrophages were seeded (with 1 × 10^5 cells) and activated with LPS (0.02 μg mL^{-1}) to create an inflamed condition, as discussed in the experimental section. Then, the secreted alkaline phosphate level (SAEP) was measured using a microplate reader at λ_{max} = 630 nm (OD). Only LPS-induced RAW 264.7 macrophage (as positive control sample) shows an OD of 2.00 ± 0.14 (a.u.). The treatment of LPS-induced RAW 264.7 macrophage (inflamed) with varying doses of Phe NPs exhibited a substantial decrease in the OD compared to the 'only LPS-induced RAW 264.7 macrophage' (as control sample). For example, upon treatment with 10, 20, 40, 100 and 150 μg mL^{-1} doses, the OD values decreased to 1.80 ± 0.20, 1.51 ± 0.27, 1.41 ± 0.40, 0.80 ± 0.21 and 0.73 ± 0.28, respectively. Therefore, with the increase in dose, a decrease in the SEAP level showed suppression in the NF-κβ level. However, beyond 40 μg mL^{-1} dose, the level decreases more than control conditions. In conclusion, Phe NPs can modulate the immune response towards anti-inflammatory directions with minimum doses and can be helpful for the inflammation-based diseases.

2.5.2. Nitric oxide (NO) release with different Phe NP doses: regulating immune and inflammatory responses. Body organ inflammation can be significantly controlled by the extent of release of NO.[39] During the inflammation process, the extent of NO production can act as a key signal. NO can contribute to inflammation or mitigate the inflammation depending on the concentration.[40] More NO can be released due to severe inflammation. Further, more inflammation caused the production of more NO by the RAW 264.7 macrophages through the enzyme nitric oxide synthase (NOS), particularly in the form of inducible NOS (iNOS) isoforms.[41] At very high levels, NO acts as a pro-inflammatory agent, and at lower concentrations, it works as an anti-inflammatory agent under physiological conditions by regulating the vascular tone and leucocyte adhesion. NO further acts as a pro-inflammatory component that influences the blood flow and cell-signalling pathways or acts as an inflammatory mediator.[42] It can also be noted that a high level of inflammation leads to the production of a high extent of NO and subsequently accelerates the organ-tissue damage through the formation of reactive nitrogen species (RNS) such as NȮ, peroxynitrite ($ONOO^-$) and the other forms of nitrogen oxides (NOx).[43] Therefore, checking the efficiency of Phe NPs in reducing the NO level under inflamed conditions is essential. Considering these issues, the RAW 264.7 macrophages have been chosen and inflamed by inducing LPS. Then, they were treated with different doses, namely, 10, 20, 40, 100 and 150 μg mL^{-1}, of Phe NPs for 24 h, and subsequently, the NO levels were estimated (Fig. 5(b)). The results reveal that LPS-induced positive control cells showed 114.36 ± 0.70% NO production with respect to RAW 264.7 macrophages (not induced by LPS), whereas, on the treatment of LPS-treated RAW 264.7 macrophages with different doses, namely, 10, 20, 40, 100, and 150 μg mL^{-1}, of Phe NPs, the NO production levels were calculated to be 104.83 ± 4.94%, 99.73 ± 6.08%, 97.58 ± 2.05%, 90.40 ± 5.02% and 75.06 ± 6.64%, respectively (Fig. 5(b)). Therefore, the NO level is suppressed with the increase in the Phe NP doses. From the results, we can conclude that Phe NPs could be used with an appropriate dose to treat inflammation.

2.5.3. RT-PCR study to estimate the immune-specific markers: Phe NP treatment on LPS induced RAW 264.7 macrophages. Semi-quantitative RT-PCR studies were conducted to determine the relative expression of genes and responses of Phe NP treatment on RAW 264.7 macrophages. The extent of Phe NPs was used in RT-PCR experiments based on the results obtained from the *in vitro* cell viability, the extent of NF-κβ, NO release and their suppression by using a dose of 50 μg mL^{-1}.

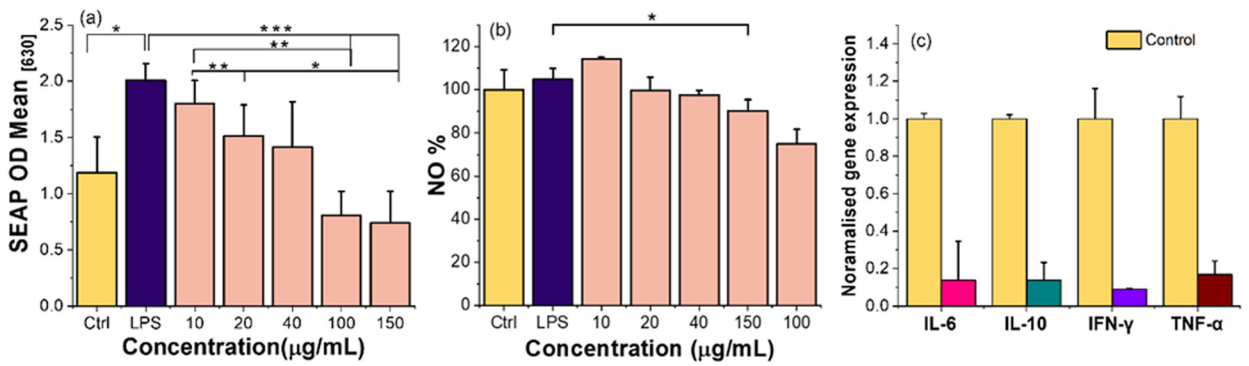

Fig. 5 RT-PCR experimental results and determination of the relative expression of genes and responses of Phe NPs against inflammation. *In vitro*, the immune response of Phe NPs was measured on an LPS-induced RAW 264.7 macrophage cell line. (a) NF-κβ Level measured by measuring SEAP levels. (b) Release of NO% under inflamed conditions and under treatment. (c) Relative expression of genes (IL-6, IL-10, IFN-γ and TNF-α), which are responsible for the body-organ inflammation and the responses of Phe NPs obtained from RT-PCR following the method explained in the experimental section. The results conclude that Phe NPs doses can control body-organ inflammation, and it is dose-dependent. *$p < 0.05$, **$p < 0.01$ and ***$p < 0.1$.

The interactions between the selected genes and the polymers were studied through *in silico* molecular docking, as mentioned in the earlier section. For RT-PCR, significant inflammation-related genes such as TNF-α, IFN-γ, IL-6 and IL-10 were selected with a control housekeeping gene (GAPDH), which are usually involved in glycolysis and other cellular processes.[44] First, the IL-6 level was measured compared to the control gene, and the results were found to be 0.139 ± 0.0.016 at 50 μg mL^{-1} dose of Phe NPs. Therefore, it can enhance the inflammatory effects by inducing the transcription factors in multiple inflammation pathways.[45] The expression of IL-6 under environmental stress such as infection can cause tissue injury.[31] However, lowering the IL-6 value under the treatment with Phe NPs is very promising to control the immune response comprising to the reduction of inflammation in different organ tissues, haematopoiesis, bone metabolism and embryonic development[46] by using an effective dose (Fig. 5(c)). Furthermore, the IL-10 level after treatment with Phe NPs was calculated, and the value was found to be 0.129 ± 0.016, which is quite lower compared to the control, signifying the regulation of immune response.

Another important pro-inflammatory cytokine is TNF-α.[47] Excess production of TNF-α induces chronic inflammatory diseases throughout the body by activating immune cells and promoting organ tissue destruction. Further, this pro-inflammatory cytokine is critical in initiating the inflammatory cascade. It has been shown to increase significantly in response to injury or infection, often correlating with other inflammatory markers.[48] After treatment with Phe NPs, the TNF-α level reaches 0.167 ± 0.016. Thus, the TNF-α level was decreased by 80% compared to the control, which is excellent evidence for reduced inflammation (Fig. 5(c)).

IFN-γ is a marker for inflammation, which is produced by the T-cells and plays a major role in cell-mediated immune responses.[49] The measuring of IFN-γ levels indicates major inflammatory diseases, Crohn's disease, autoimmune diseases and certain cancers, where excess amounts of IFN-γ worsen the patient's health conditions due to excess immune activation.[49] Therefore, the IFN-γ level was also measured using Phe NPs with a dose of 50 μg mL^{-1}, and it is observed that the IFN-γ level decreased to 0.089 ± 0.016 from the initial value of 1.00. Thus, there is 90% reduction of IFN-γ occurred comprising the activation of immune system as well as reduction of inflammation based infection (Fig. 5(c)).

2.6. Phe NPs show dose-dependent angiogenesis: studied through the *in ovo* model

Angiogenesis and inflammation are closely associated phenomena[50] as angiogenesis is triggered by immune cells during inflammation for a better supply of oxygen and nutrients. Various inflammatory disorders such as spondyloarthropathies, rheumatoid arthritis (RA) and systemic lupus erythematosus are known as angiogenic and are considered angiogenic diseases since they are associated with intensive angiogenesis. Here, it is an opportunity that if a material shows anti-inflammatory effects, then it could also work as an anti-angiogenic agent.[51] To confirm this, and from the data obtained from the MTT assay, it can be suggested that Phe NPs are biocompatible. Further, a CEMA assay was performed to check biocompatibility of Phe NPs and the angiogenic or vascular sprouting.

For this, three doses such as 1 μg, 10 μg and 100 μg of Phe NPs were used in chick embryos in triplicate, and the angiogenic properties were studied following the procedure mentioned in the method section. All the results are shown in Fig. 6, as acquired through the optical microscopy imaging process. The explant area, vessel area present and total number of junctions formed were calculated to quantify the angiogenic properties. The explant area represents the overall region, where blood vessels are developed. The explant area for the control sample increases, from 100 to 147 for 0 h to 8 h, respectively. For 1 μg and 10 μg doses, it shows a similar phenomenon, where the explant area increases from 100 to 164 and 100 to 124, respectively, for the treatment period of 0–8 h. For the dose of 100 μg, the explant area decreases from 100 for control to 91.0 for Ph NP dose (Fig. 6(b)). The vessel present area is the total surface area of blood vessels occupied in an explant area. The vessel present areas obtained for all three doses are lower in value compared to the control sample. In the junction density, a decrease in percentage (%) was observed for all the concentrations. Such as for lower concentrations of 1 μg, it shows junction density changes from 100 to 193%. For a 10 μg dose, the junction density changes from 100 to 134%; for the highest concentration of 100 μg, the value changes from 100 to 80%, whereas the reference control sample shows a value ranging from 100 to 312% (Fig. 6(d)).

All these results show that compared to control conditions; after using Phe NPs doses, no death of eggs occurred with time, which supports the MTT results. From Fig. 6, it is also noticed that there is no formation of new blood vessels compared to the control. In contrast, dose- and time-dependent variations are also noticed. At higher doses, it is becoming more anti-angiogenic. Further, it revealed that Phe NPs are anti-angiogenic in nature at higher concentrations, and the results further support the anti-inflammatory behaviour of Phe NPs.

2.7. Phe NPs are hemocompatible: studied on RBCs

A crucial aspect for developing effective nanomedicines is its hemocompatibility, or the ability of nanoparticles to interact with blood without causing adverse toxic effects, such as clotting of blood, disrupting the natural angulation mechanism and impairing the fibrinolytic system severely.[52,53] Poor hemocompatibility may cause inflammation and it takes a longer time for therapy. Thus, understanding the dose-dependent hemolysis of Phe NPs is very important. To check this, the hemocompatibility of Phe NPs was studied *in vivo* in a rat model. For a substance to have a better therapeutic impact, hemolysis should be less than 5%.[54] Fig. 7(a) shows the hemocompatibility results, featuring the microcentrifuge tubes displaying hemolysis (%) at 4 h and 8 h using the dose ranges

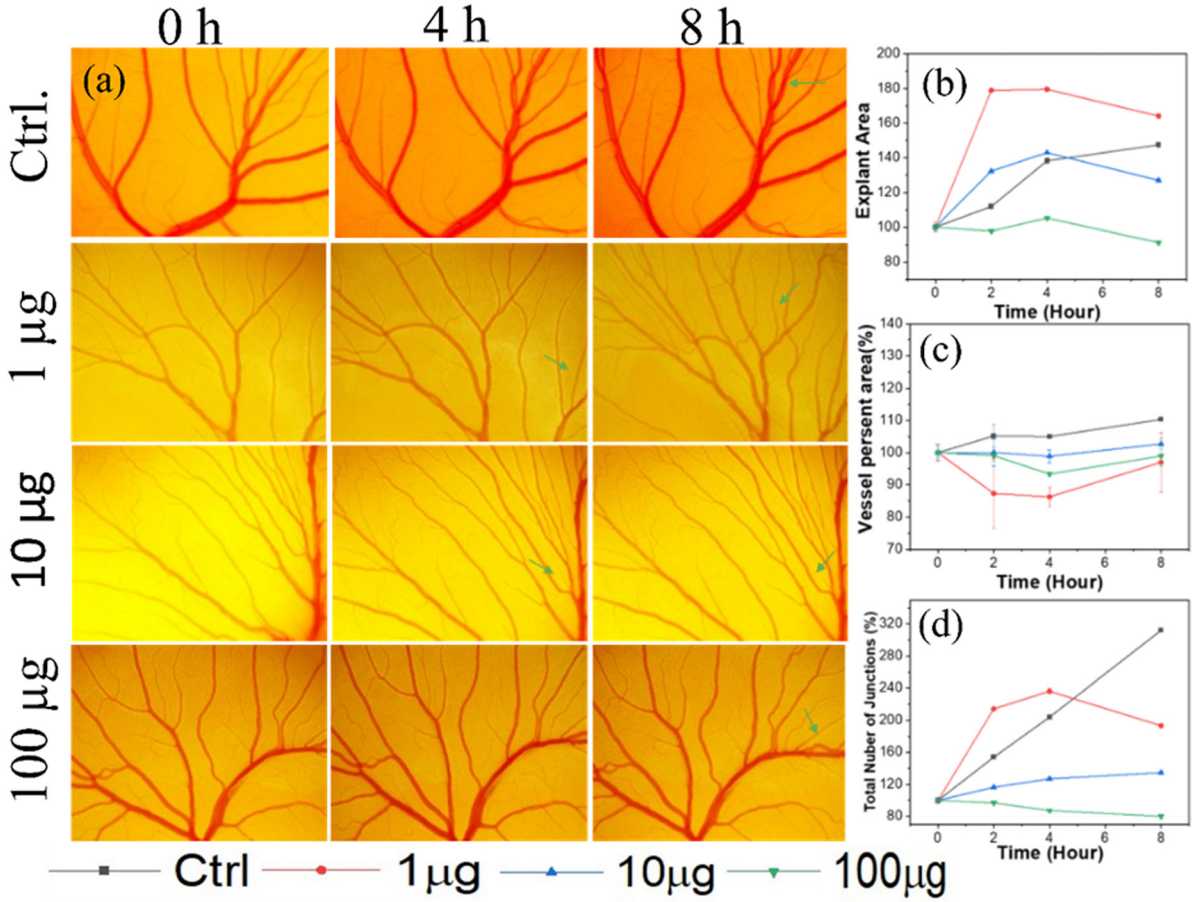

Fig. 6 Angiogenesis results obtained for Phe NPs. Microscopy images were obtained for the control sample and different doses (1 µg, 10 µg and 100 µg) of Phe NPs. (a) Dose-dependent angiogenesis at different periods of treatment, revealing the dose-dependent morphological changes in egg blood vessels. (b) Explant area at different doses and periods. (c) Change in the area of vessels with different doses and treatment periods. (d) Total number of the junctions generated with different doses and periods. All the results were compared with the results obtained from the control experiment.

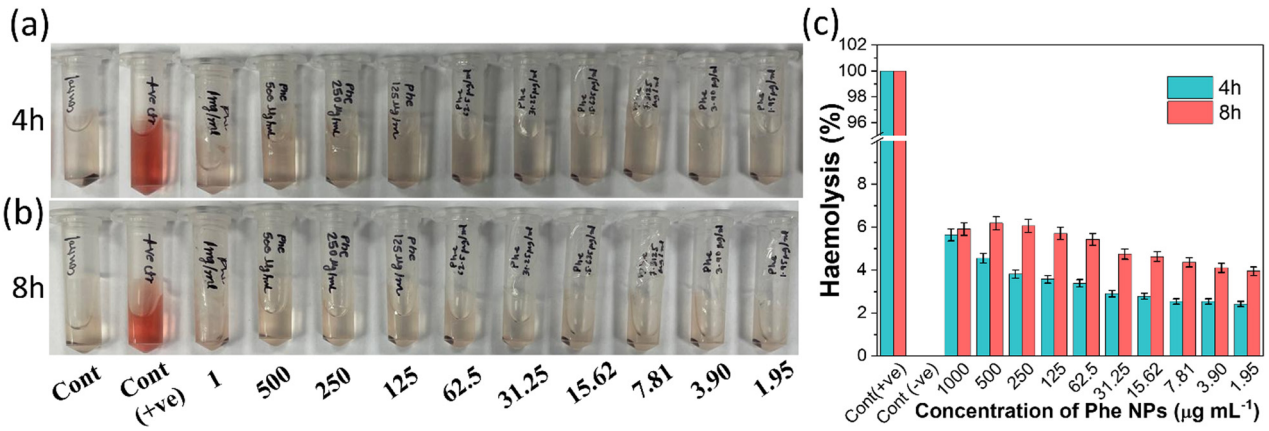

Fig. 7 Hemocompatibility analysis for Phe NPs with different doses. (a) and (b) Representative camera images taken for the microcentrifuge tubes showing hemolysis at 4 h and 8 h. (c) Hemolysis (%) of Phe NPs with different doses against rat erythrocytes. The results show that Phe NPs are hemocompatible in nature.

from a minimum of 1.95 µg mL^{-1} to a maximum of 1 mg mL^{-1} of blood sample. Hemolyis for control sample was considered 100%. The hemolysis for all the doses was found to be less than 5% (Fig. 7), confirming that the Phe NPs are hemocompatible.

2.8. Anti-inflammatory and immune protective responses of Phe NPs: studied using an *in vivo* LPS-induced systemic rat model

The *in vivo* potential of Phe NPs was assessed using an LPS-induced systemic rat paradigm. After LPS injection, large amounts of pro-inflammatory cytokines can be identified in the circulating serum.[55] An *in vivo* rat model was developed using male Wistar rats to check the anti-inflammatory and immune-protective responses of Phe NPs, as mentioned in the experimental section. The details of the *in vivo* protocols are shown in Fig. 8(a and b). The results are segregated according to the study into different parts, represented in Fig. 8(c) and explained in the subsequent sections.

2.8.1. Systemic anti-inflammatory responses of Phe NPs: concluded through blood-based biochemical parameters. To assess the systemic inflammation, the levels of biochemical markers such as CRP,[56] lactate[57] and procalcitonin (PCT) were estimated.[58] At 0 h, 6 h, 18 h and 30 h, the collected blood samples were checked for CRP, lactate and procalcitonin levels.

CRP. CRP is an acute-phase protein that increases significantly in response to inflammation. It is a sensitive biomarker for detecting inflammatory states including infections and tissue injury.[59] CRP levels typically rise within 6 h after the onset of inflammation, peaking around 24–48 h, and may remain elevated for several days depending on the severity of the inflammatory response. The obtained CRP level for G1 (control) is 100 ± 6.34% at 0 h and remained the same even at 30 h. For G2 (positive control), initially (at 0 h) the CRP level was 100.00 ± 3.88%, and after 6 h of LPS incubation, it reached 153.10 ± 3.33%, which further increased to 158.47 ± 3.20% and 159.32 ± 2.31% at 18 h and 30 h, respectively. For G3, *i.e.*, after treatment with 0.1 mg of Phe NPs per kilogram of body weight, the CRP level changes from normalized 100 ± 4.04% to 145.30 ± 0.84% (after 6 h of LPS treatment). Then, the Phe NP treatment was performed and the CRP levels were estimated at 12 and 24 h post-treatment, and the values obtained were 124.93 ± 3.24% and 110.72 ± 1.82%, respectively. For G4, the CRP level changes from normalized 100 ± 2.39% to 142.14 ± 1.46% (after 6 h of LPS treatment). Then the Phe NP treatment was performed (*i.e.*, after treatment with 1 mg of Phe NPs per kilogram of body weight of rat), and the CRP levels were estimated at 12 and 24 h post-treatment and the values were determined to be 107.59 ± 8.29% and 101.57 ± 2.48%, respectively.

For G5, the CRP level changes from 100 ± 3.19% to 147.94 ± 3.42% (after 6 h of LPS treatment). Then, Phe NP treatment was performed (*i.e.*, after treatment with 10 mg of Phe NPs per kilogram of body weight of rat), and the CRP levels were estimated at 12 and 24 h post-treatment and the values were determined to be 112.13 ± 1.77% and 107.91 ± 4.17%, respectively. Therefore, it is evident that the CPR level generated

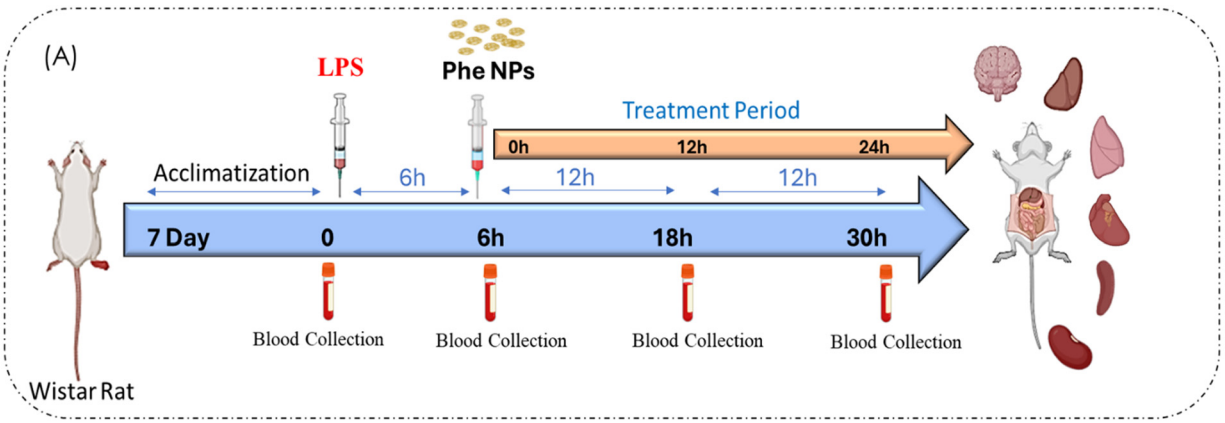

(B)

Animal Groups	Conditions
Control (G1)	Control
Positive Control (G2)	LPS (1mg/kg)
Dose-1 (G3)	LPS + Phe NPs (0.1mg/Kg)
Dose-2 (G4)	LPS + Phe NPs (1 mg/Kg)
Dose-3 (G5)	LPS + Phe NPs (10 mg/Kg)

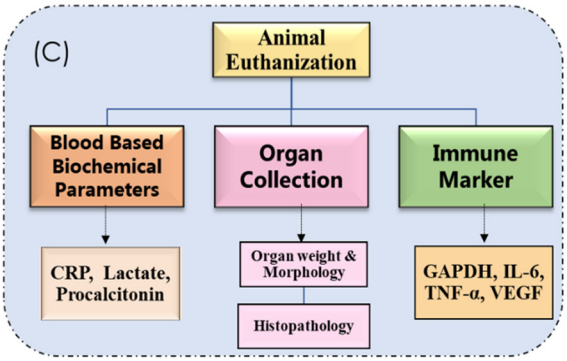

Fig. 8 The details of *in vivo* experiments designed to study the anti-inflammation effect of Phe NPs. (a) Time-dependent *in vivo* study for inflammation generation and treatment with Phe NPs and organ-based treatment plans. (b) The different groups of rats taken for treatment and (c) the whole experimental plans after treatment and the plan for measuring biochemical parameters.

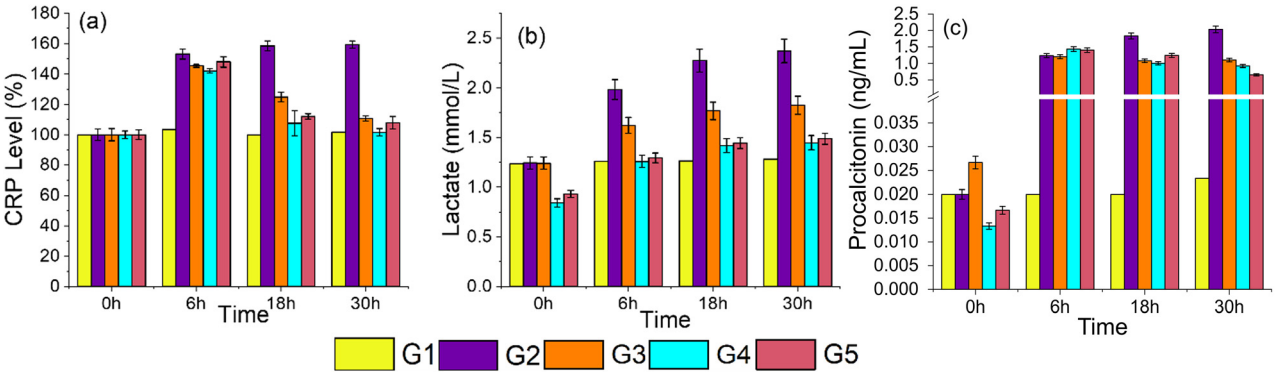

Fig. 9 Estimated results of blood-based biochemical parameters of all the groups of rats at different time points. (a) CRP level (%), (b) lactate level (mmol L^{-1}), and (c) procalcitonin (ng mL^{-1}) at different periods post-treatment. The *p*-values are mentioned in Table S3. *$p < 0.05$, **$p < 0.01$ and ***$p < 0.1$.

under inflammation can be reduced by treating with Phe NPs and the extent of inflammation suppression and efficiency of protection could be firmly controlled by the doses of Phe NPs used (see Fig. 9(a)).

Lactate. Lactate levels can indicate tissue hypoxia and are often elevated during systemic inflammatory responses due to increased anaerobic metabolism. Elevated lactate levels can be observed within a few hours of the onset of systemic inflammation and are used to assess the severity of the inflammatory response.[57]

The lactate levels for G1 (control) were determined to be 1.236 ± 0.041 mmol L^{-1} at 0 h and 1.28 ± 0.01 mmol L^{-1} at 30 h. For G2 (positive control), initially (at 0 h) the lactate level was 1.24 ± 0.06 mmol L^{-1}. After 6 h of LPS incubation, it reached 1.98 ± 0.09 mmol L^{-1} which further increased to 2.27 ± 0.11 mmol L^{-1} and 2.37 ± 0.11 mmol L^{-1} at 18 h and 30 h post-treatment, respectively. For G3, *i.e.* after treatment with 0.1 mg of Phe NPs per kilogram of body weight, the lactate level changes from 1.24 ± 0.06 mmol L^{-1} to 1.62 ± 0.08 mmol L^{-1} (after 6 h of LPS treatment). After treatment with Phe NPs, the lactate levels were estimated at 12 and 24 h post-treatment to be 1.76 ± 0.08 mmol L^{-1} and 1.82 ± 0.09 mmol L^{-1}, respectively. For G4, the lactate level changes from 0.84 ± 0.04 mmol L^{-1} to 1.25 ± 0.06 mmol L^{-1} (after 6 h of LPS treatment). After treatment with 1 mg of Phe NPs per kilogram of body weight of rat, the lactate levels were estimated at 12 and 24 h post-treatment to be 1.41 ± 0.06 mmol L^{-1} and 1.44 ± 0.07 mmol L^{-1}, respectively.

For G5, the lactate level changes from 0.93 ± 0.03 mmol L^{-1} to 1.29 ± 0.04 mmol L^{-1} (after 6 h of LPS treatment). After treatment with 10 mg of Phe NPs per kilogram of body weight of rat, the lactate levels were estimated at 12 and 24 h post-treatment to be 1.44 ± 0.05 mmol L^{-1} and 1.48 ± 0.05 mmol L^{-1}, respectively. Therefore, it is evident that the treatment of Phe NPs can reduce the lactate level generated under inflammation, and the extent of inflammation suppression and efficiency of protection is strongly controlled by the doses of Phe NPs used (Fig. 9(b)).

Procalcitonin (PCT). PCT is a precursor of calcitonin that acts as a marker for bacterial infection and systemic inflammation. Its levels increased rapidly in response to pro-inflammatory stimuli, particularly during bacterial infections.[59] The PCT level is known to increase more rapidly than CRP often within 6 h post-inflammation induction, making it as a valuable marker for early diagnosis of sepsis.[60]

The obtained PCT levels for G1 (control) are considered to be 0.02 ± 0.001 ng mL^{-1} at 0 h, and they remained the same even at 30 h. For G2 (positive control), initially (at 0 h) the PCT level was 0.02 ± 0.001 ng mL^{-1}, and after 6 h of LPS injection, the value increased to 1.23 ± 0.06 ng mL^{-1}, which further changes to 1.83 ± 0.09 ng mL^{-1} and 2.03 ± 0.10 ng mL^{-1} at 18 h and 30 h post-treatment, respectively. For G3, *i.e.*, after treatment with 0.1 mg of Phe NPs per kilogram of body weight, the PCT level changes from 0.02 ± 0.001 ng mL^{-1} to 1.2 ± 0.06 ng mL^{-1} (after 6 h of LPS treatment). The PCT levels were estimated to be 1.07 ± 0.05 ng mL^{-1} and 1.1 ± 0.05 ng mL^{-1} at 12 and 24 h post-treatment with Phe NPs, respectively. For G4, the PCT level changes from normalized 0.01 ± 0.006 ng mL^{-1} to 1.43 ± 0.07 ng mL^{-1} (after 6 h of LPS treatment). After treatment with 1 mg of Phe NPs per kilogram of body weight of rat, the PCT levels were estimated at 12 and 24 h post-treatment to be 1.0 ± 0.05 ng mL^{-1} and 0.92 ± 0.04 ng mL^{-1}, respectively.

For G5, the PCT level changes from 0.01 ± 0.0008 ng mL^{-1} to 1.4 ± 0.07 ng mL^{-1} (after 6 h of LPS treatment). After treatment with 10 mg of Phe NPs per kilogram of body weight of rat, the PCT levels were estimated at 12 and 24 h post-treatment to be 1.24 ± 0.06 ng mL^{-1} and 0.65 ± 0.03 ng mL^{-1}, respectively. Therefore, it is evident that the treatment of Phe NPs can control the PCT level generated under inflammation conditions, and the extent of inflammation suppression and efficiency of protection can be effectively controlled by the doses of Phe NPs used (Fig. 9(c)).

Monitoring these biomarkers over the time period, they provide valuable insights into the progression of the treatment of systemic inflammation and can guide to take clinical decision-making regarding treatment strategies. Elevated levels of CRP and PCT are particularly indicative of ongoing infection

or severe inflammatory responses. At the same time, lactate is an essential marker for assessing tissue perfusion and metabolic status during inflammation. Serum PCT, CRP and lactic acid levels increase in response to infection and high levels have been found to be correlated with the severity of infection, the development of MODS and the worse outcomes in various infectious diseases.[61]

2.8.2. Systemic anti-inflammatory responses of Phe NPs: studied by measuring the weights of organs and their morphologies. Systemic inflammation can cause an increase in the body and organ weight. Subsequently, an increase in body-organ weight impairs the production of leptin, a hormone that regulates the appetite and metabolism.[62] Therefore, checking the body-organ weight after creating inflammation in rats with LPS and after treatment of Phe NPs at different doses is essential. Further, the histological changes of the organs are also crucial for understanding the effects of inflammation on various organs.[63] Following euthanasia, each rat's body weight and organ-to-body weight ratios were calculated. Key organs such as the liver, kidneys, spleen, heart and lungs were excised carefully. Each organ is rinsed with saline to remove blood and debris and then blotted dry with filter paper to measure the weights. Then, the organ-to-body weight ratio was calculated using eqn (1):

$$\text{Organ to body weight ratio} = (\text{Weight of organ})/(\text{Body weight}) \times 100 \quad (1)$$

Lungs. LPS administration led to significant pulmonary oedema as is evidenced by an increased wet-to-dry weight ratio of lung tissue. This suggests considerable fluid accumulation due to inflammation and disruption of the alveolar-capillary barrier, which leads to fluid leaking into the lung tissue.[64] This condition affects the lung-to-body weight ratio indirectly through increased fluid retention.[65] From Fig. 10(a–c) and Tables S4, S5, it is evident that the lung's weight increases for G1 (control) to G2 (positive control, LPS induced, inflamed) from 1.33 ± 0.11 g to 2.1 ± 0.1 g, respectively. However, once G2 was treated with Phe NPs, *i.e.*, for G3 (0.1 mg kg^{-1}), G4 (1 mg kg^{-1}), and G5 (10 mg kg^{-1}), the lungs weight changed from 2.1 ± 0.1 g to 1.5 ± 0.1 g, 1.6 ± 0.1 g and 1.8 ± 0.1 g, respectively. Further, the details about the change in the lung weight/body weight are shown in Fig. 10(a–c), which clearly implies that the lung weight increased due to the inflammation induced by LPS and reduced after treatment with Phe NPs, and that the treatment efficiency could be controlled in a dose-dependent manner.

Kidney. The inflammation in the kidney causes nephritis. Nephritis can be caused by the infection, autoimmune disorder or by toxins. Nephritis is of different types such as glomerulonephritis (inflammation in the glomeruli causing swelling and fatigue), interstitial nephritis (inflammation surrounding the tubules causing fever and discharge of blood in urine) and tubulitis (inflammation in the renal tubules).[66] Nephritis can affect one or both kidneys. Finally, the kidneys showed signs of damage, which finally required dialysis and kidney transplantation if it failed. Therefore, the study highlighted that LPS caused acute kidney injury, which further can typically correlate with the kidney weight relative to the body weight over time. From Fig. 10(a, b and d) and Tables S4, S5, it is evident that the kidney weight increases for G1 (control) to G2 (positive control, LPS induced and inflamed) from 1.16 ± 0.60 g to 1.53 ± 0.15 g, respectively. However, once G2 was treated with Phe NPs, *i.e.*, for G3 (0.1 mg kg^{-1} body weight), G4 (1 mg kg^{-1} body weight) and G5 (10 mg kg^{-1} body weight), the kidney weight changed from 1.53 ± 0.15 g to 1.2 ± 0.1 g, 1.3 ± 0.26 g, and 1.13 ± 0.11 g, respectively. Further, the details about the change in the ratio of kidney weight/body weight are shown in Fig. 10(d), which clearly implies that the kidney weight increased due to the inflammation induced by LPS, which could be reduced by the treatment with Phe NPs. However, the treatment efficiency could be controlled in a dose-dependent manner.

Liver. There are various reasons for liver inflammation such as parasites and viruses, which may cause liver damage.[67] Further, chronic liver inflammation causes fibrosis, cirrhosis and many cases of cancer.[67] As mentioned earlier, LPS alters innate immunity and causes inflammation by producing proinflammatory cytokines, chemokines, ROS or NO, which can further generate inflammation in the liver. While specific liver weight data were not highlighted, it can be noted that LPS treatment significantly altered the liver morphology or weight within the 24-h timeframe.[68] Therefore, the study highlighted that LPS caused acute liver inflammation, which typically may correlate with the liver weight relative to body weight over time under the treatment with Phe NPs. From Fig. 10(a, b and e) and Tables S4, S5, it is evident that the liver weight increases for G1 (control) to G2 (positive control, LPS induced, inflamed) from 6.83 ± 3.5 g to 8.13 ± 0.25 g, respectively. However, once G2 was treated with Phe NPs, *i.e.*, for G3 (0.1 mg kg^{-1} body weight), G4 (1 mg kg^{-1} body weight), and G5 (10 mg kg^{-1} body weight), the liver weight changed from 8.13 ± 0.25 g to 7.7 ± 0.2 g, 7.06 ± 0.15 g and 7.23 ± 0.25 g, respectively. Further, the details about the change in the ratio of liver weight/body weight are shown in Fig. 10(e). It is evident that the liver weight increases due to the inflammation induced by LPS, which could be reduced by treatment with Phe NPs and the treatment efficiency could be controlled in a dose-dependent manner.

Spleen. The inflammation of the spleen can cause increased levels of inflammatory cytokines such as IL-1β, IL-6, IL-10, and TNF-γ.[69] It is reported in the earlier section that the inflammatory cytokine levels have already increased, and by the treatment with Phe NPs, their levels can be reduced. However, there is a notable increase in spleen weight (splenomegaly) and the spleen-to-body weight ratio following LPS administration, which suggests the activation of the immune response and splenic proliferation.[70] This increase indicates splenic hyperplasia due to immune activation in response to LPS administration.[70]

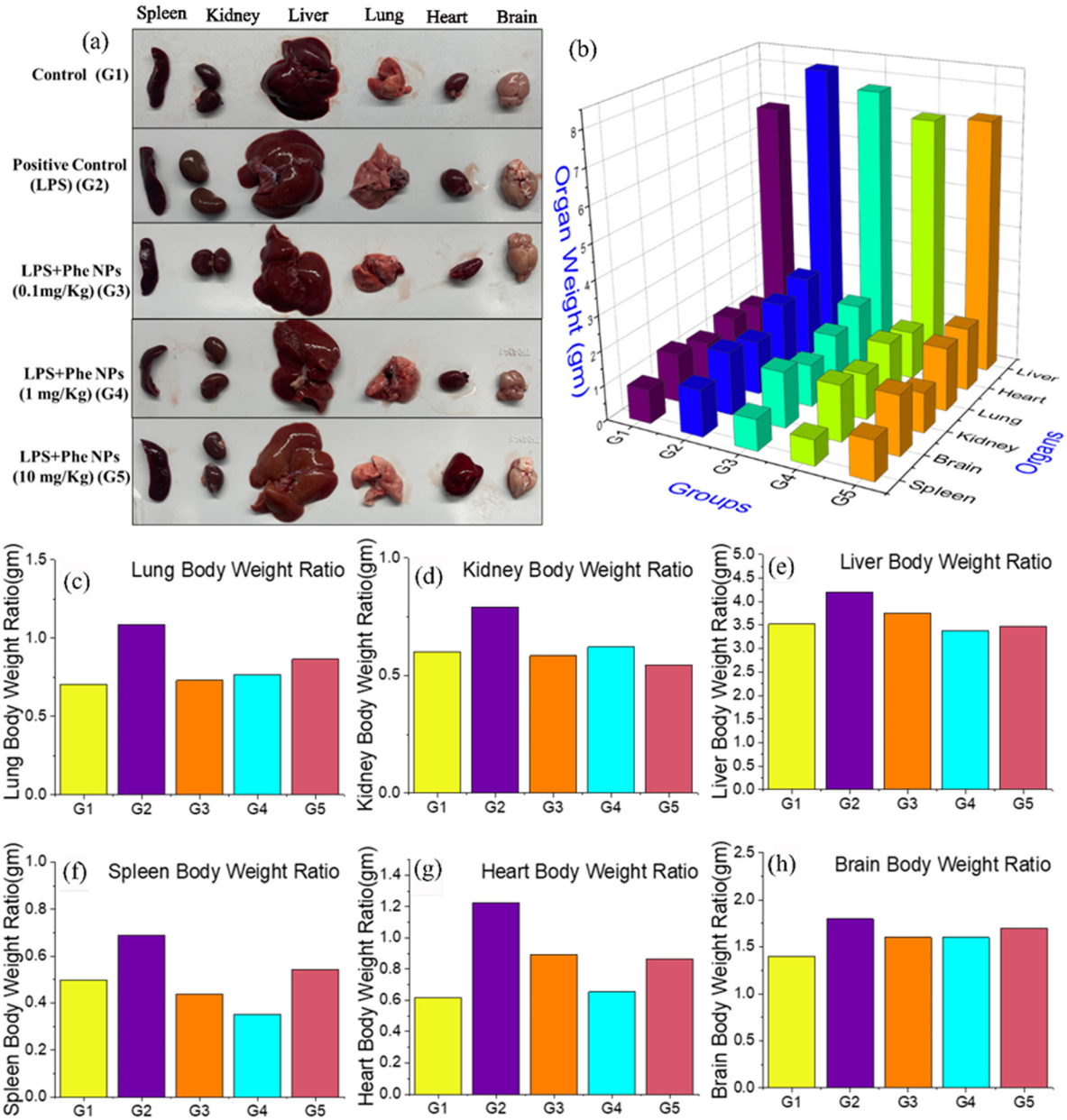

Fig. 10 (a) Camera photos of isolated organs showing their morphology. (b) Organ weight of different groups of rats for different organs. (c) Lung-to-body weight ratio, (d) kidney-to-body weight ratio, (e) liver-to-body weight ratio, (f) spleen-to-body weight ratio, (g) heart-to-body weight ratio and (h) brain-to-body weight ratio.

From Fig. 10(a, b and f) and Tables S4, S5, it is evident that the spleen weight increases for G1 (control) to G2 (positive control, LPS-induced, inflamed) from 0.96 ± 0.20 g to 1.33 ± 0.15 g, respectively. However, once G2 was treated with Phe NPs, *i.e.*, for G3 (0.1 mg kg^{-1} body weight), G4 (1 mg kg^{-1} body weight) and G5 (10 mg kg^{-1} body weight), the spleen weight changed from 1.33 ± 0.15 g to 0.9 ± 0.1 g, 0.73 ± 0.15 g and 1.13 ± 0.15 g, respectively. Further, the details about the change in the spleen weight/body weight ratio are shown in Fig. 10(f). These results clearly implied that the spleen weight increased due to the inflammation induced by LPS, which could be reduced by the treatment with Phe NPs.

Heart. Inflammation causes an increase in weight as oedema occurs in response to stress on the cardiovascular system, potentially affecting heart function and structure.[71] The weight of the G1 group rats, which are the control rats, means ± S.D. value is 1.2 ± 0.2 g. However, after LPS induction, the positive control group (G2) rats show an increase in their weight of 2.36 ± 0.15 g. For G3 (0.1 mg kg^{-1} body weight), G4 (1 mg kg^{-1} body weight) and G5 (10 mg kg^{-1} body weight), the heart weight changed to 1.83 ± 0.20 g, 1.36 ± 0.68 g and 1.8 ± 0.1 g, respectively. Further, the details about the change in the heart weight/body weight ratio are shown in Fig. 10(g), which implies that the heart weight increased due to the inflammation

induced by LPS, which could be reduced by the treatment with Phe NPs (0.1 and 1 mg kg^{-1} doses). In contrast, with the highest concentration of Phe NPs, the heart weight increased more than that under the control condition, showing that the treatment efficiency could be controlled in a dose-dependent manner (Fig. 10(a, b and g) and Tables S4, S5).

Brain. Neuroinflammation causes many inflammatory diseases.[72] The study indicated that LPS treatment resulted in changes in brain tissue, including neuronal degeneration and a thinner cell layer in the hippocampus. LPS treatment stimulates microglia through the activation of NF-κβ.[73] However, the search results did not provide specific quantitative data on brain weight. Therefore, the study highlighted that LPS caused acute neuroinflammation, which typically can be correlated with the weight of brain relative to body weight over the time period under the treatment of Phe NPs.

From Fig. 10(a, b and h) and Tables S4, S5, it is evident that the weight of brain increases for G1 (control) to G2 (positive control, LPS induced and inflamed) from 1.4 ± 0.1 g to 1.8 ± 0.1 g, respectively. However, once G2 was treated with Phe NPs, *i.e.*, for G3 (0.1 mg kg^{-1} body weight), G4 (1 mg kg^{-1} body weight), and G5 (10 mg kg^{-1} body weight), the brain weight changed from 1.8 ± 0.1 g to 1.6 ± 0.1 g, 1.6 ± 0.1 g and 1.7 ± 0.1 g, respectively. Further, the details about the change in the brain weight/body weight ratio are shown in Fig. 10(e), which implies that the weight of the brain increased due to the inflammation induced by LPS, and NPs could reduce the inflammation in a dose-dependent manner.

2.8.3. Anti-inflammatory responses of Phe NPs: studied through histological analysis of systemic organs. Infections and injury might trigger the systemic inflammatory response syndrome (SIRS) and tissue damage. Endotoxin, particularly LPS, is a key factor in inducing severe and systemic inflammatory responses during sepsis and acute tissue damage in multiple organs such as the lung, liver, kidney, spleen, heart and brain. First, we examined the potential of LPS in inflammation and tissue damage in LPS-challenged rats, and then treatment was performed. After the completion of the treatment period, we euthanized the rats. Then, the different tissues were dissected out and examined by histopathology. H&E staining was carried out in other tissues (kidney, lung, liver, brain, heart and spleen) to find aberrant histopathological alterations in the vital organs, and the results are shown in Fig. 11.

The histological slices of the lungs of the control rats (G1 or A1) showed a normal alveolus and the interstitium was free from cell infiltration, as indicated by the green arrow, indicating the absence of inflammatory cells. In LPS-induced lung tissue (G2 or A2), the thickness of the alveolar wall was increased and the number of pulmonary alveoli was reduced by LPS injection. The treatment of LPS boosted the infiltration of inflammatory cells, which induce tissue damage in the lung. The black arrow highlights the damage sites of infiltration of inflammatory cells and thickening of the alveolar wall. No significant changes were observed in lung tissue when the rats were administered with 0.1 mg Phe NPs dose (G3 or A3) for 24 h. In contrast, treatment with a higher dose, *i.e.*, 10 mg Phe NPs (G5 or A5) for 24 h, significantly alleviates the extent of tissue damage and reduces the lung inflammation. The administration of Phe NPs further suppressed the swelling of the alveolar wall and decreased the number of lung alveoli in LPS-challenged rats. The green arrows are pointed to the undamaged sites, inflammatory cells and repressed swelling of the alveolar wall (Fig. 11A1–A5).

The kidneys of untreated groups (G1 or B1) showed normal-shaped renal tubules, glomerulus and Bowman's capsules, with no tissue damage. However, LPS administration (G2 or B2) markedly increased the infiltration of inflammatory cells in the kidney. Renal tubular epithelial cells were sloughed and brush borders and renal epithelial cells were decreased after LPS injection. Black arrows are pointed to the areas of injury and inflammatory cell infiltration. However, the administration of Phe NPs (10 mg Phe NPs) (G5 or B5) inhibited the inflammatory cell infiltration, sloughing of tubular epithelial cells and diminished brush borders and epithelial cells in the kidney, as indicated by the green arrow (Fig. 11B1–B5).

Liver tissues appeared normal, with no evidence of vascular changes and hepatocellular damage in the control rat (G1 or C1). However, when rats were administered with LPS (G2 or C2), it showed liver damage. LPS-induced injury markedly increased hepatocyte damage and inflammatory cell infiltration in the liver, ultimately manifesting as liver inflammation. Damage sites, inflammatory cell infiltration and hepatocyte damage are indicated by the black arrow. However, 10 mg Phe-NP (G5 or C5) treatment inhibited the infiltration of inflammatory cells into the cavities of liver tissue, which was caused by LPS as seen by the green arrows (Fig. 11C1–C5).

The spleen from untreated mice (G1 or D1) revealed no evidence of vascular change, lymphoid follicular damage, typical white pulp lymphatic nodules, red pulp splenic cords and the spleen trabecula. Following an LPS injection in rats (G2 or D2), we observed changes in the histological structure of the spleen, including that the red pulps are intensely congested with red hemolyzed cells. The volume fraction of white pulp and lymphoid follicles was increased. The black arrow highlights congested red hemolyzed cells, infiltrating inflammatory cells, and damaged areas. Conversely, 10 mg Phe NP-treated spleen (G5 or D5) revealed typical white pulp lymphatic nodules, red pulp splenic cords and spleen trabeculae, as indicated by the green arrows, affirming that the Phe NPs are safer and devoid of organ toxicity (Fig. 11D1–D5).

The cross-sectional histological examination of the control heart (G1 or E1) showed no signs of vascular change, myofiber damage, and normal cardiomyocyte structure with a single, oval and centrally placed nucleus, as indicated by the green arrows. In contrast, inflammatory cell infiltrates were increased, and disarrangement was observed in the LPS-induced damaged heart, as pointed by the black arrow (G2 or E2). However, the administration of Phe NPs exhibited a trend of improvement in histological changes in the heart tissue. The rats treated with 10 mg Phe NPs (G5 or E5) also had a normal cardiomyocyte structure with a single, oval and centrally placed nucleus

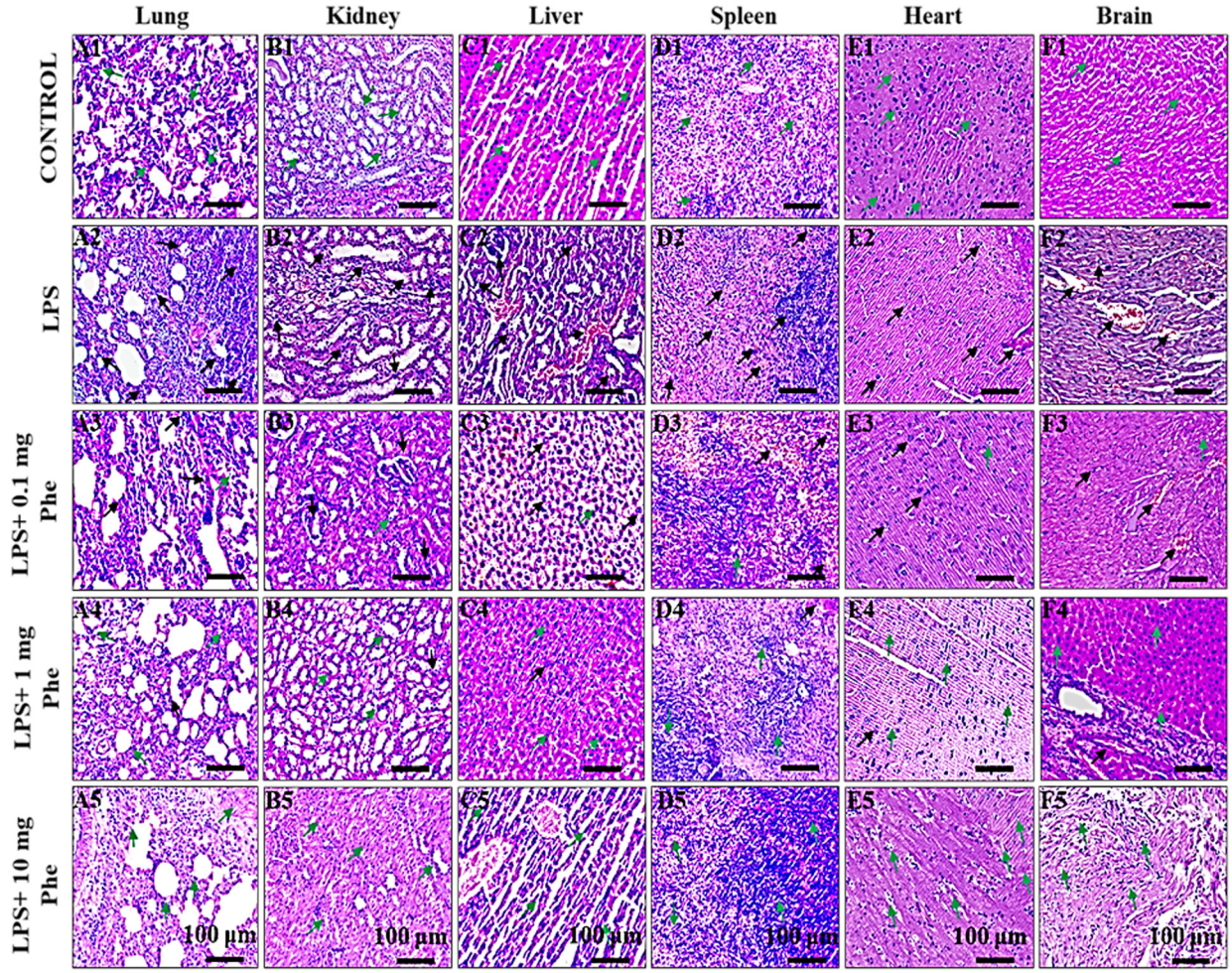

Fig. 11 H&E analysis of Phe NP-treated damaged lung, kidney, liver, spleen, heart and brain tissues in LPS-challenged Wistar rats. Male Wistar rats were injected with PBS (vehicle), LPS (200 µg kg^{-1}, i.p.) and different concentrations of Phe NPs (0.1 mg kg^{-1}, 1 mg kg^{-1}, and 10 mg kg^{-1}, i.v.) as mentioned in the Materials and methods section (A1: control, A2: LPS, A3: LPS + 0.1 mg kg^{-1} Phe NPs, A4: LPS + 1 mg kg^{-1} Phe-NPs, A5: LPS + 10 mg kg^{-1} Phe NPs in lung tissue; B1–B5 in the kidney; C1–C5 in the liver; D1–D5 in the spleen; E1–E5 in the heart; and F1–F5 in the spleen, respectively). The lung, kidney, liver, spleen, heart, and brain tissues were harvested after the treatment period. The results show H&E staining of the lung, kidney, liver, spleen, heart and brain tissue sections from the indicated group (20×). The black arrow indicates the damaged sites and infiltration of inflammatory cells. The green arrow points to the normal cells and undamaged sites. The scale bar is 100 µm for all the images. The figure is representative of three independent experiments.

uniformly arranged with myofibrils, which was similar to the control rat, as highlighted by the green arrows (Fig. 11E1–E5).

H&E staining of the brain tissue of control rats (G1 or F1) showed dense, purplish-blue nuclei and large pyramidal cells in the cytoplasm of neurons with no damage, as indicated by the green arrow. At 30 h post-LPS injection (G2 or F2), noticeable neuronal damage was observed in the brain. In the LPS group, the cells became swollen and abnormally circular, and increased neuronal loss and neuronal vacuolation occurred in the cortex region of the brain. The black arrows highlighted the vascular congestion, vacuolation, inflammatory cells and damaged area. However, this inflammatory response and tissue damage were reduced over time in the Phe NP-treated group of rats. Treatment with 10 mg Phe NPs (G5 or F5) has shown a reduction in neuronal loss in the brain in 24 h time period. The green arrows show normal, dense, purplish-blue nuclei and large pyramidal cells in the cytoplasm of neurons. The green arrow shows normal, dense, purplish-blue nuclei and large pyramidal cells in the cytoplasm of neurons (Fig. 11F1–F5). LPS plays a role in the aetiology of sepsis by stimulating immunological responses, resulting in tissue destruction and multiple organ failure. Thus, treatment with Phe NPs reduced the infiltration of inflammatory cells and tissue damage in the lung, liver, kidney, spleen, heart and brain and enhanced the survival rate of LPS-challenged rats.

2.8.4. Systemic anti-inflammatory responses of Phe NPs studied on LPS-induced rats: relative expression of immune markers. In the context of systemic inflammation induced by LPS in rats, evaluating immune markers such as IL-6, vascular endothelial growth factor (VEGF) and TNF-α using RT-PCR provides insight into the molecular response to inflammation. Relative expression values of these immune markers were checked from blood samples collected at 24 h post-treatment.

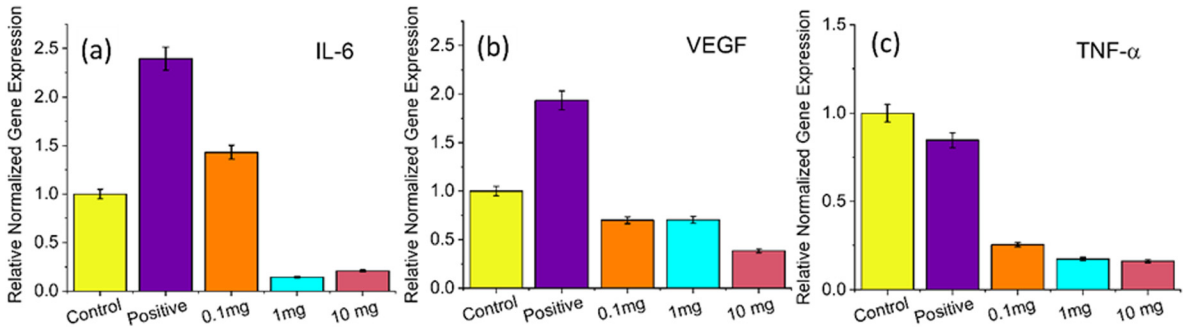

Fig. 12 Immune RT-PCR-based assessment of Phe NPs after 30 h of incubation in rat blood. (a) Relative normalized gene expression of IL-6, (b) relative normalized gene expression of VEGF, and (c) relative normalized gene expression of TNF-α.

The IL-6 expression level is normalized by using GAPDH as a control gene. Fig. 12(a) shows the results for the control group (G1), where the IL-6 level reaches 1.00 ± 0.05. For the positive control group G2, it reaches 2.39 ± 0.11. After treatment with 0.1 mg kg^{-1} weight of rat (G3), the IL-6 level is suppressed to 1.43 ± 0.07, for G4 (treatment with 1 mg kg^{-1} weight of rat), it is highly suppressed to 0.14 ± 0.007, and for the treatment with 10 mg kg^{-1} weight of rat (G4), the IL-6 level is changed to 0.21 ± 0.01. From the angiogenesis results, it is evident that Phe NPs are antiangiogenic in nature. Therefore, it is very important to check the expression level of VEGF, since it is a growth factor responsible for the formation of vessels.[74] The VEGF expression level is normalized using GAPDH as a control gene. Fig. 12(b) shows the results for control group (G1), exhibiting the VEGF level of 1.00 ± 0.05, and in the positive control group (G2), the VEGF level reaches 1.93 ± 0.09, whereas after treatment with 0.1 mg kg^{-1} weight of rat (G2), the VEGF level is reduced to 0.69 ± 0.03, after treatment with 1 mg kg^{-1} weight of rat (G4), it changes to 0.70 ± 0.03, and for treatment with 10 mg kg^{-1} weight of rat (G5), the VEGF level changes to 0.38 ± 0.01. Therefore, the highest level of VEGF suppression is shown after treatment with Phe NPs in the rat model.

It is important to check the level of TNF-α after treatment with Phe NPs. Control (G1) shows a TNF-α level of 1.00 ± 0.05. In the positive control group (G2), the TNF-α level reaches 0.84 ± 0.04, whereas for treatment with 0.1 mg kg^{-1} (G3), the TNF-α level is suppressed to 0.25 ± 0.01 and for the G4 (treatment with 1 mg kg^{-1}), it is suppressed to 0.17 ± 0.008 and for G5 (treatment with 10 mg kg^{-1}), the TNF-α level changes to 0.16 ± 0.008. Therefore, the highest level of suppression of TNF-α is seen after treatment with Phe NPs (Fig. 12(c)).

3. Conclusions

Systemic inflammation can lead to single or multi-organ failure, septic shock or severe infection and even mortality if treatments are not provided. Researchers are making attempts to develop new anti-inflammatory drugs to prevent the adverse biological effects of the existing therapies. In this work, we have synthesized amino acid-based polymeric nanoparticles (Phe NPs) using *N*-acryloyl chloride and *N*-acryloyl-L-phenylalanine methyl ester. The biological and immune roles have been assayed using immune cells. Then, *in silico* docking was performed to know the interactions of the various components responsible for inflammation and the possible role of the novel polymeric nanoparticles in controlling their levels. Further, *in vitro* and *in vivo* studies were performed to check the role of Phe NPs in reducing systemic inflammation. LPS-stimulated RAW 264.7 macrophages were used *in vitro* and an LPS-induced rat model was used to check the anti-inflammatory responses of Phe NPs. The results obtained from both types of studies are very promising, and it is revealed that the treatment efficiency depends on the doses of Phe NPs. The anti-inflammatory response of Phe NPs was checked by RT-PCR analysis using different doses with the inflamed markers TNF-α, IFN-γ, IL-6 and IL-10. Finally, the rats were sacrificed, their systemic organs (brain, liver, kidneys, spleen, lungs and heart) were harvested followed by the determination of their weight, and real-time images were acquired. The collected organs were subjected to full H&E histological analysis. Their histological analysis evaluated the severity of inflammation and the response of Phe NPs with different dosages on specific organs. Finally, it can be concluded that amino acid-based Phe NPs have a huge scope in controlling systemic inflammation. Specifically, the study revealed that the Phe NPs are immune adjuvants with anti-inflammatory and anti-angiogenic properties even at a low concentration. The future scope for this study is to check this nanoparticle with anti-inflammatory drugs to reveal their synergistic approach, and this NP could become a supporting therapy for terminally ill patients for their continuous organ failure due to inflammation. Further, clinical research could be conducted to determine the end uses of these unique Phe NPs.

4. Experimental

4.1. Materials and methods

Commercially available materials were used to synthesize the required polymer. L-Phenylalanine methyl ester hydrochloride (99%) (Sigma-Aldrich, 7524-50-7), acryloyl chloride (96%) stabilized with 400 ppm phenothiazines (Thermofisher scientific, 814-68-6), hexadecane (anhydrous) (99%) (Sigma-Aldrich, 544-76-3),

and divinyl benzene (DVB) (Sigma-Aldrich,1321-74-0) were used in this experiment. Chloroform (SRL, 67-66-3), ethyl acetate (Sigma-Aldrich,141-78-6), 1,4-dioxane (>99% pure) (Sigma-Aldrich, 123-91-1), 2,2-azobisisobutyronitrile (AIBN) (SRL; >98%), SDS (>90%, Merck), dichloromethane, *N*-hexane, DMEM, fetal bovine serum, penicillin–streptomycin cocktail and DAPI (Invitrogen, D1306) were also used. All samples were prepared using ultrapure water (18.2 MΩ cm^{-1}) obtained from a Pure Lab Ultra water system by ELGA in High Wycombe. Methyl thiazole tetrazolium (MTT ≥99.9%) was obtained from Himedia. The Quanti Blue (Invitrogen), Griess reagent (Biotium, 30100), LPS (Sigma L2880) and the specified testing kits were obtained commercially and experiments were performed as per the manufacturers guidelines. Sisco Research Laboratories Pvt. Ltd, Mumbai, India, provided analytical grade reagents without additional purification needs.

4.2. Synthesis of the *N*-acryloyl-L-phenylalanine methyl ester monomer (Phe Monomer)

A modified method from our previously reported work[23] was followed for the synthesis of the *N*-acryloyl-L-phenylalanine monomer.[75] In brief, L-phenylalanine methyl ester hydrochloride (2.15 g) with trimethylamine (1.6 mL) was dissolved in 60 mL ice-cold dry DCM in a round-bottom flask on ice (Solution A). In another flask, 0.9 mL of acryloyl chloride and 5 mL of DCM were taken in an ice bath (Solution B). Solution B was added dropwise to Solution A and stirred overnight at room temperature. After evaporating the solvents in a high vacuum, the residue was dissolved in 100 mL of ethyl acetate. The resulting solution was washed several times with $NaHCO_3$, $NaHSO_4$ and brine solutions. Magnesium sulphate was used before drying using a Rota-evaporator. The final step involved either column chromatography or hexane trituration for purification. This process gave 76% yield of the monomer.

4.3. Synthesis of poly(*N*-acryloyl L-phenylalanine methyl ester) nanoparticles (Phe NPs)

Following our earlier works, the mini-emulsion free radical polymerization method was used to obtain poly(*N*-acryloyl-L-phenylalanine methyl ester) nanoparticles (Phe NPs),[23] with modifications according to the need.[76] To synthesize the Phe NPs, a freshly prepared 500 mg monomer was dissolved in 2 mL of toluene for 30 min. At each 10-min interval, 10 mg hexadecane, 20 mg DVB and 10 mg initiator [2,2-azobisisobutyronitrile (AIBN)] were added with continuous stirring (Solution A). The whole mixture was bath sonicated for 3 min. Then, in another bottle, 30 mg of sodium dodecyl sulphate (SDS) was dissolved in 8 mL water and added to Solution A. Then, this mixture was ultra-probe sonicated (at 750 W and 30% power) on ice for another 3 min. Then, the mixture was transferred to a 50 mL round-bottom flask and stirred for 24 h at 75 °C with vigorous stirring to convert the monomers into polymers over the oil droplets. To evaporate toluene after 24 h, the mixture was shifted to a 100 ml round-bottom flask, and 10 mL of water was added to it and stirred for 24 h at 85 °C. Finally, SDS was removed by repeated washing with a mixture of water and isopropanol (3 : 1) through centrifugation (at 10 000 rpm).

4.4. Characterization

The chemical functionality of the Phe monomers and Phe NPs was investigated using ^{1}H-NMR and ^{13}C-NMR (AVH D 500 AVANCE III HD 500 MHz OneBay NMR Spectrometer, BRUKER BioSpin INTERNATIONAL AG) spectrometers (500 MHz) with a deuterated solvent ($CDCl_3$) at 25 °C using tetramethyl silane as an internal standard in NMR. Solid-state NMR/13CP Mass Experiment was performed using a Neo 600 MHz, Bruker, Switzerland; Probe: PH MAS DVT 600S3 BL 3.2 N-P/F-H. The functional groups were identified by FTIR spectroscopy (Nicolet iS5, 4 Thermo Fisher Scientific Inc., USA) using a KBr pellet. The size, shape and morphology of the nanoparticles were estimated by HRTEM (Tecnai G2 20 TWIN, FEI Company of USA (S.E.A.) PTE, LTD). For reconfirming the HRTEM results and understanding the morphology of NPs, AFM (NTEGRA Prima, NT-MDT Service & Logistics Ltd) was performed. The average particle size and zeta potential (ζ) were determined by dynamic light scattering (DLS; Nano-ZS ZEN3600, Malvern, UK) at 25 °C in PBS (pH 7.4).

4.5. *In vitro* cell viability of Phe NPs

In vitro experiments were conducted to assess the biocompatibility and immune response of Phe NPs. The initial screening involved a cell viability assay across multiple cell lines including fibroblasts (L929), human embryonic kidney cells (HEK-293), glioblastoma cells (PC-12) and RAW264.7 macrophages, which were selected for their importance in viability and immune response. All cell lines were acquired from NCCS, Pune, India. The culture medium for these experiments contained Dulbecco's modified Eagle's medium (DMEM), supplemented with 10% fetal bovine serum (FBA) and 1% antibiotics, namely penicillin and streptomycin cocktail.

The cells were incubated at 37 °C in a 5% CO_2 environment, with the culture medium being replaced every two days. The MTT assay follows an identical protocol for all cell lines to assess cell viability. In the experimental setup, cells were seeded into 96-well plates at a density of 5000 cells per well and incubated for 24 h at 37 °C with 5% CO_2 to facilitate adherence to the healthy surfaces. Subsequently, different concentrations of Phe NPs of 1 μg mL^{-1} to 1000 μg mL^{-1} were taken with cells. The Phe NPs were incubated for 24 h and then an MTT solution (5 mg mL^{-1} dissolved in PBS) was added. The volume was made up with complete DMEM media followed by incubation at 37 °C for 4 h. The final step involved removing the MTT mixture, adding 100 μL of DMSO to each well in dark and incubating for 30 min. The absorbance of the 96-well plate was acquired at 570 nm using a UV-Vis spectrophotometer. The percentage of cell viability (%) was calculated using eqn (2):

$$\text{Cell viability (\%)} = \frac{\text{OD (treatment)}}{\text{OD (control)}} \times 100 \quad \text{OD} = \text{Optical density.} \tag{2}$$

2.6. *In vitro* cellular uptake by confocal microscopy and flow cytometry (FACS)

To investigate the cellular uptake of Phe NPs, we explicitly selected immunological RAW 264.7 macrophages. The RAW

264.7 macrophages were seeded on lysine-coated glass coverslips in 6-well plates at a density of 1×10^6 cells per well, containing 2 mL of complete media. After 24 h of incubation, the cells reached 70–80% confluence and adhered to the surface. The NPs were prepared and labelled with Nile red, followed by 24 h incubation. Subsequently, the Nile red-stained Phe NPs suspended in complete media at a concentration of 100 μg mL^{-1} were added to cells and incubated for another 24 h. Following this, the cells were washed three times with PBS (pH 7.4) to eliminate unbound Phe NPs. The cells were then fixed using 400 μL of 4% paraformaldehyde solution per well for 30 min. After fixation, the cells underwent DAPI staining. Each coverslip was mounted onto a glass slide using Dabco as the mounting medium. The distribution of Phe NPs within the cells was identified using a Leica Super-resolution SP8 confocal microscope (BHU-SATHI). The resulting images were analysed using the Leica and Image J Fiji Software.

Additionally, a flow cytometry experiment was conducted to reconfirm the cellular uptake of Phe NPs quantitatively. The cells were seeded in a 6-well culture plate (Corning, USA) at a density of 3×10^4 cells per well and incubated at 37 °C overnight. Then, Phe NPs with 100 μg mL^{-1} were added and incubated for 24 h. The cells were washed twice with 1 mL of PBS to remove residual NPs and harvested in PBS. Then, the cell suspension was collected by centrifugation at 12 000 RPM for 5 min. The cells were kept at 4 °C until the flow cytometry experiment was conducted. Fluorescence signals indicate the cellular uptake of Rhodamine-labelled Phe NPs using a flow cytometer (model: FACS Verse, BD Biosciences).

2.7. Molecular docking study with Phe and inflammation-targeted protein receptors

Before the *in vitro* analysis of inflamed specific markers, *in silico* docking studies were performed. The molecular docking studies were conducted with specific inflammation-targeted protein receptors. The targeted gene was sorted out following the procedure previously reported in the literature. The well-known commercially available drug IBF was selected as a control to compare the docking results with Phe NPs. The following are the significant steps used for docking; (a) protein preparation: for docking, the receptors selected are IL-6 (pdb id 1ALU), NF-κβ (pdb id 1VKX), TNF-α (2AZ5), COX2 (pdb id 3LN1) and IL-1β (pdb id 5I1B). The 3D structures of the chosen receptors were retrieved from the RCSB protein Data Bank (**https://www.rcsb.org/**). Subsequently, water molecules were removed using Autodock 1.5.6 by adding polar hydrogen and Kollman's charges. The resulting proteins were then saved in PDBQT format. The second step is (b) Ligand Preparation: the ligands selected were ibuprofen (IBF) and phenylalanine (Phe). Their 3D structures were acquired from PubChem in the SDF file format. Then, this SDF file was converted into PDB using Discovery Studio. Further, 'pdbqt' files for the ligands were generated by Pymol. A similar method was followed for *N*-acryloyl phenylalanine. The next step is (c) grid generation and docking analysis. Following the preparation of ligands and proteins, the molecular docking was conducted using Autodock (1.5.6). A grid with dimensions less than 1 Å specific to *X*, *Y*, and *Z* coordinates was established to encompass the protein, as here we performed the blind docking. This grid was centred around the protein to facilitate the most feasible docking conformations. Subsequently, the grid file was saved as a (.gpf) file. Then the autogrid was initiated. The calculations were then performed using the Lamarckian genetic algorithm (GA), which fixed 50 runs. The files were saved as '.pdf'. After running AutoDock, the final docking results were obtained in the 'dlg' file format that showed H-bonding, binding energy and inhibition constants. The best docking conformation of the ligand with the receptors was selected based on the estimated binding energy (E_g) and inhibition constant (K_i). The protein–ligand complex with the lowest binding energy was extracted in the PDBQT format. Further, the interactions between ligands and proteins of these complexes were extracted using LigPlot+, Autodock and ChimeraX in 2D and 3D.

4.8. Estimation of the *in vitro* NF-κβ levels for regulating inflammatory responses

For the immune screening of Phe NPs, the NF-κβ level was measured. NF-κβ is a crucial transcription factor significantly regulating inflammatory responses. It expresses various pro-inflammatory genes including cytokines and chemokines that are essential for immune responses.[77] To check the NF-κβ level, RAW 264.7 macrophage cells were seeded (1×10^5 cells) in 96-well plates after 24 h of incubation of cells. The cells are activated with LPS (0.2 μg mL^{-1}) to create inflamed conditions other than a control group of cells. After incubation for 24 h with LPS, the Phe NPs with different doses (10, 20, 40, 100 and 150 μg mL^{-1}) were used for the treatment. The treatment was scheduled for 24 h. Then, a well-prepared QB solution of 180 μL and the cell supernatant of 20 μL were added to another 96-well culture plate. The prepared solution was incubated for 2 h in the dark at 37 °C. The secreted alkaline phosphate level (SAEP) was measured using a microplate reader at λ_{max} = 630 nm OD. A Quanti Blue solution was prepared with 1 mL of QB reagent and 1 mL of QB Buffer in 98 mL sterile water following the manufacturer's protocol (InvivoGen).

4.9. Estimation of the *in vitro* NO levels for regulating immune and inflammatory responses

Nitric oxide (NO) is a critical signalling molecule involved in various physiological processes, and it can be produced by various immune cells including macrophages and neutrophils. As a signalling molecule, NO influences several activities that modulate inflammatory responses.[78] Therefore, the response of Phe NPs for the production of NO by RAW 264.7 cells was estimated using the Griess reagent [1% (w/v)] and sulphadiazine mixed with 0.1% (w/v) *N*-naphthyl ethylenediamine dihydrochloride (1 : 1), by measuring the nitrite concentration. RAW 264.7 macrophage cells were cultured in 96-well plates at a density of 2×10^5 cells per well for 24 h at 37 °C and 5% CO_2. To find out whether the NPs could inhibit LPS-stimulated NO production or not, the cells were treated with different doses of Phe NPs (10, 20, 40, 100 and 150 μg mL^{-1}), diluted in the cell

culture medium. After 24 h of incubation, 100 μL of cell supernatant was collected and plated in another 96-well plate alongside an equal volume of the Griess Reagent. The absorbance (Abs) of the samples was measured at 550 nm.

4.10. *In vitro* immune screening of Phe NPs by RT-PCR

The *in vitro* immune response of Phe NPs was confirmed by performing an RT-PCR study with the marker specified in the literature and through *in silico* molecular docking. This study selected significant inflammation-related genes such as TNF-α, IFN-γ, IL-6 and IL-10 with GAPDH as the control housekeeping gene. For this study, RAW 264.7 macrophages were seeded in 12-well plates, where LPS (0.2 μg mL^{-1}) was used to induce cell inflammation. After 24 h, cells were treated with 100 μg mL^{-1} of Phe NPs from this cell suspension. The total RNA content was extracted using TRIZOL following the manufacturer's guidelines (Thermofisher). The RNA concentration and purity were measured using a NanoDrop spectrophotometer (Thermo Fisher Scientific). RT PCR was performed using 1 μg of RNA and a High-Capacity cDNA Reverse Transcription Kit (Applied Biosystems, USA) in a 20 μL reaction mixture. PCR amplification was carried out using specific primers (mentioned in S-1). The reverse transcription conditions were 95 °C for 2 min. The RT enzyme activity was kept at 95 °C for 10 s. The denaturation and melting were performed at 65–95 °C at a heating rate of 0.5° min^{-1}. The process was continued 39 times, and the melting profile was acquired between 65 °C and 95 °C (with 0.5 °C per 5 s heating rate). The gene-specific primers were amplified using a thermal cycler (Bio-Rad, Base Serial No. CT058999, Optical Head Serial No. 785BR31742).

4.11. Chicken embryo membrane assay (CEMA) for assessing the angiogenic properties of Phe NPs

Fertilized chicken eggs were acquired from a reliable and licensed vendor (Ramana Hatchery, Varanasi, Uttar Pradesh, India) and incubated in an egg incubator (37 °C, 50–55% Relative humidity) for up to 4 days before the experiment. On the day of the experiment, the eggs were examined by a light-shadow method to see if embryogenesis had happened. The chick embryo's chorioallantoic membrane was then detached by eliminating 1–2 mL of albumen using injection, and a small window was created on the eggshell. The Phe NPs were dispersed in PBS (pH 7.41) at various doses (1, 10 and 100 μg). PBS was used as a control and examined for up to 24 h. The images of the embryo were acquired at multiple time intervals (0, 2, 4, and 8 h) using a stereo zoom microscope-mounted camera (Magcam DC Plus 10, Magnus Opto Systems India Pvt. Ltd), featuring a 10-megapixel resolution. The images were analysed using the Angio tool and Fiji Image J software.

4.12. Hemocompatibility of Phe NPs

To find out the hemocompatibility of Phe NPs, a hemolysis study was carried out with the red blood cells of rats. First, a rat cardiac puncture was made to collect blood. After resuspension, blood was centrifuged at 3500 rpm for 5 min at 25 °C to obtain a consistent suspension of RBCs in sterile DNS (5×10^6 cells μL^{-1}). RBCs were treated with Phe NPs at different concentrations (1 mg mL^{-1} to 1.95 μg mL^{-1}) for 2 h, 8 h and 24 h at 37 °C and kept at 100 rpm in an incubator shaker. DNS and pure water were used as negative and positive controls, respectively. Then, the samples were collected and centrifuged again at 3500 rpm for 5 min at 25 °C. The supernatant was collected, the absorbance was measured at λ_{max} = 540 nm and the percentage of hemolysis was calculated using the eqn (3):

$$\text{Hemocompatibility (\%)} = \frac{\text{OD (treatmet)} - \text{OD(negative control)}}{\text{OD(positive control)} - \text{OD(negative control)}} \times 100$$

$$\text{OD} = \text{Optical density.} \quad (3)$$

All the experiments were conducted in triplicates.

4.13 *In vivo* anti-inflammation behaviour of Phe NPs: LPS-induced systemic inflammation model

An LPS-induced systemic rat inflammation model was developed to examine the anti-inflammatory response of Phe NPs *in vivo*.[79] The LPS animal model has several significant advantages including technical simplicity and high reproducibility, especially regarding the induced inflammatory response. After LPS administration, a high extent of proinflammatory cytokines can be released, which can be measured in the circulating serum.[80] All *in vivo* studies were performed on 8 to 12-week-old male Wistar rats. For this study, 15 rats weighing 185-225 g each were taken by maintaining the cage body mass and divided into five different groups, as shown in Fig. 8(b). Artificial light was turned on from 07:00 a.m. to 07:00 p.m., the room temperature was maintained at 22 ± 1 °C and the relative humidity was 50 ± 5%. Isoflurane was used for anaesthesia during the inflammation study to minimize stress.

A 24-h systemic rat inflammation study was conducted, as illustrated in the accompanying scheme in Fig. 8(a). Blood samples were collected at designated time intervals, starting from 0 h for biochemical analysis including CRP, lactate and procalcitonin levels. Immediately after blood sample collection, an intraperitoneal injection of LPS was administered to all animals except the sham control group. At 6 h after LPS induction, blood was drawn from all the animals to determine whether inflammatory conditions were developed or not. As the biochemical markers indicated inflammation, all rats were treated with three different dosages of Phe NPs, namely, 0.1 mg kg^{-1}, 1 mg kg^{-1} and 10 mg kg^{-1}.

For G1 (sham control), the animals were injected with an equal volume of saline. G2 (positive control, LPS-induced) remained unchanged since it was a positive control group, only with an induced inflammatory condition. For G3, the rats were injected with the lowest Phe NPs (1 mg kg^{-1}). For G4, the dose was 1 mg kg^{-1} of Phe NPs, and for G5 (shown in Fig. 8(b)), the maximum dose was 10 mg kg^{-1} of Phe NPs.

The study was conducted for 30 h, where the initial 6 h were taken for developing LPS-induced inflammation and the

subsequent 24 h for Phe NP treatment. Blood samples were collected from all the animals at different time points (0 h, 6 h, 18 h and 30 h) (shown in Fig. 8(a)). In the end, all the rats were euthanized, and their systemic body organs such as the brain, liver, lung, kidney, heart, and spleen were collected for weighing individually (Fig. 8(c)). All the collected organs and blood samples were processed for further studies (Fig. 8(c)).

4.13.1. Assessment of biochemical parameters responsible for inflammation. The blood was collected every alternate hour in the LPS-induced systemic inflammatory model. Blood-based biochemical parameters were checked to evaluate infection-based inflammation and sepsis. The significant parameters secreted in the initial hours are CRP, lactate and procalcitonin. The C-reactive protein (CRP) level was measured following the immunoturbidimetry method (CRP Turbilatex) as per the manufacturer's protocol. The lactate level was measured using a Lactate estimation kit (GenX Lactate) following the LOX-PAP method on photometric systems as per the manufacturer's protocol (Proton, PBLAC25), and the procalcitonin level was measured from blood serum at room temperature (25 °C).

4.13.2. *In vivo* immune marker analysis by RT-PCR. Blood samples were collected *via* cardiac puncture at 30 h post-LPS administration and 24 h of Phe NPs induction. Blood was immediately transferred into EDTA tubes to prevent clotting, and the blood samples were centrifuged at 3000 rpm for 10 min to separate plasma from cellular components. The PBMC layer was collected and washed with phosphate-buffered saline (PBS) to remove the residual medium. The triazole-based RNA extraction method was used to isolate the total RNA. The RNA concentration was quantified and the purity was assessed using a Nanodrop. Extracted RNA was converted to complementary DNA (cDNA) using a reverse transcription kit (Thermo Fisher Scientific), following the manufacturer's instructions for optimal conditions. A reaction mixture containing specific primers for TNF-α, IL-6 and VEGF and a housekeeping gene (*e.g.*, GAPDH) as a control was prepared. The RT-qPCR reactions were carried out in a 96-well plate according to the established protocols, as mentioned in the *in vitro* RT-PCR section, ensuring that each sample was run in triplicates for accuracy. The experiments were conducted using a real-time PCR machine, setting appropriate cycling conditions based on the primer specifications. Fluorescence was monitored at each cycle to determine every target gene's threshold cycle (Ct) values.

4.13.3. Histopathological study (H&E staining): anti-inflammatory analysis of Wistar rat tissues. H&E staining analysis is one of the best ways to evaluate the inflammatory/anti-inflammatory properties of medicines.[81] To validate our *in vitro* observations as an anti-inflammatory property of Phe NPs, an *in vivo* rat model was developed using male Wistar rats, as discussed earlier. At the end of the treatment, all the rats were euthanized. The systemic organs (brain, heart, lungs, liver, kidneys and spleen) were harvested, immediately fixed with 4% formalin solution and then embedded with paraffin. The tissues were sliced and stained with hematoxylin and eosin (H&E) and examined using a microscope to detect any abnormal histopathological changes in the vital organs. For H&E staining, paraffin-embedded specimens were cut into sections of 5 μm thickness, mounted on slides and heated at 60 °C for 30–40 min. After deparaffinization with xylene, the sections were rehydrated by submerging them in alcohol of different concentrations (100%, 90%, 70%, and 50%, respectively). Then, the slides were immersed in hematoxylin followed by eosin stain (H&E) and rinsed carefully in water. Then, slides were dehydrated by immersing in increasing alcohol concentrations of 50%, 70%, 90%, and 100% and, finally, incubated in xylene for 2 min. The sections were mounted using a mounting solution. Images were acquired at 20×/40× magnifications using a bright-field microscope (Magcam DC Plus 10, Magnus Opto Systems India Pvt. Ltd).

4.14. Biosafety/ethical permission

All the *in vivo* studies were conducted according to the guidelines of the Institutional Animal Ethical Committee (IAEC) of the Indian Institute of Technology (IIT), Banaras Hindu University, Varanasi (Registration no. 2123/GO/Re/S/21/CPCSEA) with approval (IAEC Approval No. IIT(BHU)/IAEC/2024/II/028, dated 13/09/2024).

4.15. Statistical significance

One-way ANOVA with independent Student's *t*-test was used to evaluate the statistical errors and significance of *in vitro*, *in ovo and in vivo* results using the Origin software (Origin Lab Corporations, Northampton, USA). The statistical significance in comparison groups was calculated considering $^{*}p < 0.05$, $^{**}p < 0.01$ and $^{***}p < 0.1$. The data are represented as mean ± SD, unless otherwise stated.

Author contributions

P. Paik is the principal project investigator (PI). Ideation, major experimental design, experimental results analysis, and manuscript writing were performed by D. Pareek and P. Paik, Y. Mastai helped in the synthesis, characterization and explanation of results. S. Patra, G. Singh, K. Wasnik, Aman S Kudada and Rajalaxmi Pradhan helped in characterization. Taniya Das and Anjali R. Mourya helped in molecular docking. Md. Zeyaullah and Prakriti S. Samanta helped in *in vivo* work. The manuscript was written and finalized by D. Pareek and P. Paik. All the authors checked and approved the manuscript for publication.

Conflicts of interest

There are no conflicts of interest to declare.

Data availability

All the data will be available from the corresponding author/1st author as required.

Fig. S1 and S2: NMR (^{1}H and ^{13}C) of the monomer; Fig. S3: solid-state NMR/13CP mass experiment data of the polymer of *N*-acryloyl-L-phenylalanine; Fig. S4: AutoDock binding energy

comparison of IBF and Phe. Table S1: all docking binding energy and inhibition constants; Table S2: primer details on RT PCR; Table S3: statistical analysis of blood-based biochemical parameters data; Tables S4 and S5: different organ weights for all the experimental groups and individual rat data for body weight, organ weight and organ-to-body weight ratios. See DOI: https://doi.org/10.1039/d5tb00886g

Acknowledgements

The authors acknowledge the financial support awarded to Prof. Paik by the I-DAPT foundation (Ref. I-DAPT/IT (BHU)/2023-24/Project Sanction/47), Indian Council of Medical Research (ICMR), India (Ref: EMDR/SG/12/2023-4724); STARS-IISc. Bangalore (Ref. MoE-STARS/STARS-2/2023-0318) and Anusandhan National Research Foundation (ANRF), India (Ref: CRG/2023/005576). The authors also acknowledge the Start-up company Triphan Healthcare Pvt. Ltd, at I3F, IIT(BHU), Varanasi, India, for instrumental supports. D. Pareek acknowledges the DST-INSPIRE fellowship awarded to carry out the PhD work (Ref. IF 180928).

References

1 M. Drozd, M. Pujades-Rodriguez, A. W. Morgan, P. J. Lillie, K. K. Witte, M. T. Kearney and R. M. Cubbon, *J. Infect. Dis.*, 2022, **226**, 554–562.
2 D. Furman, J. Campisi, E. Verdin, P. Carrera-Bastos, S. Targ, C. Franceschi, L. Ferrucci, D. W. Gilroy, A. Fasano, G. W. Miller, A. H. Miller, A. Mantovani, C. M. Weyand, N. Barzilai, J. J. Goronzy, T. A. Rando, R. B. Effros, A. Lucia, N. Kleinstreuer and G. M. Slavich, *Nat. Med.*, 2019, **25**, 1822–1832.
3 A. Menzel, H. Samouda, F. Dohet, S. Loap, M. S. Ellulu and T. Bohn, *Antioxidants*, 2021, **10**, 414.
4 R. Sohail, M. Mathew, K. K. Patel, S. A. Reddy, Z. Haider, M. Naria, A. Habib, Z. U. Abdin, W. Razzaq Chaudhry and A. Akbar, *Cureus*, 2023, **15**, e37080.
5 T. J. Yoo, *J. Alzheimer's Dis.*, 2022, **85**, 1001–1008.
6 S. L. Navarro, E. D. Kantor, X. Song, G. L. Milne, J. W. Lampe, M. Kratz and E. White, *Cancer Epidemiol., Biomarkers Prev.*, 2016, **25**, 521–531.
7 R. Ohno and A. Nakamura, *Semin. Arthritis Rheum.*, 2024, **67**, 152479.
8 N. K. Panchal and E. Prince Sabina, *Food Chem. Toxicol.*, 2023, **172**, 113598.
9 L. Wang, B. Zhu, Y. Deng, T. Li, Q. Tian, Z. Yuan, L. Ma, C. Cheng, Q. Guo and L. Qiu, *Adv. Funct. Mater.*, 2021, **31**, 2101804.
10 M. C. Martínez and R. Andriantsitohaina, *Antioxid. Redox Signaling*, 2008, **11**, 669–702.
11 Z. Tu, Y. Zhong, H. Hu, D. Shao, R. Haag, M. Schirner, J. Lee, B. Sullenger and K. W. Leong, *Nat. Rev. Mater.*, 2022, **7**, 557–574.
12 Y. Huang, X. Guo, Y. Wu, X. Chen, L. Feng, N. Xie and G. Shen, *Signal Transduction Targeted Ther.*, 2024, **9**, 34.
13 L. Liu, X. Bai, M.-V. Martikainen, A. Kårlund, M. Roponen, W. Xu, G. Hu, E. Tasciotti and V.-P. Lehto, *Nat. Commun.*, 2021, **12**, 5726.
14 M. Khoshnamvand, Z. Hao, O. O. Fadare, P. Hanachi, Y. Chen and J. Liu, *Chemosphere*, 2020, **258**, 127346.
15 R. I. Lynch and E. C. Lavelle, *Biochem. Pharmacol.*, 2022, **197**, 114890.
16 A. N. Galindo, D. A. Frey Rubio and M. H. Hettiaratchi, *Mater. Adv.*, 2024, **5**, 4025–4054.
17 R. Brusini, M. Varna and P. Couvreur, *Adv. Drug Delivery Rev.*, 2020, **157**, 161–178.
18 R. Aquilani, G. C. Zuccarelli, R. Maestri, M. Boselli, M. Dossena, E. Baldissarro, F. Boschi, D. Buonocore and M. Verri, *Int. J. Immunopathol. Pharmacol.*, 2021, **35**, 20587384211036823.
19 D. Pareek, M. Zeyaullah, S. Patra, O. Alagu, G. Singh, K. Wasnik, P. S. Gupta and P. Paik, *J. Mater. Chem. B*, 2025, **13**, 3094–3113.
20 R. Lev and W. C. Griffiths, *Gastroenterology*, 1982, **82**, 1427–1435.
21 A. C. L. Leite, F. F. Barbosa, M. V. D. O. Cardoso, D. R. M. Moreira, L. C. D. Coêlho, E. B. da Silva, G. B. D. O. Filho, V. M. O. de Souza, V. R. A. Pereira, L. de, C. Reis, P. M. P. Ferreira, C. Pessoa, A. G. Wanderley, F. V. B. Mota and T. G. da Silva, *Med. Chem. Res.*, 2014, **23**, 1701–1708.
22 Y. Gonda, A. Matsuda, K. Adachi, C. Ishii, M. Suzuki, A. Osaki, M. Mita, N. Nishizaki, Y. Ohtomo, T. Shimizu, M. Yasui, K. Hamase and J. Sasabe, *Proc. Natl. Acad. Sci. U. S. A.*, 2023, **120**, e2300817120.
23 A. K. Yamala, V. Nadella, Y. Mastai, H. Prakash and P. Paik, *Nanoscale*, 2017, **9**, 14006–14014.
24 S. Patra, Jyotirmayee, K. Kumar, D. Pareek, P. S. Gupta, A. R. Mourya, T. Das, K. Wasnik, M. Verma, R. Chawla, T. Batra and P. Paik, *J. Mater. Chem. B*, 2025, **13**, 3876–3894.
25 J. Skey and R. K. O'Reilly, *J. Polym. Sci., Part A: Polym. Chem.*, 2008, **46**, 3690–3702.
26 S. Mazumdar, D. Chitkara and A. Mittal, *Acta Pharm. Sin. B*, 2021, **11**, 903–924.
27 Y. Ysrafil, Z. Sapiun, N. S. Slamet, F. Mohamad, H. Hartati, S. A. Damiti, F. D. Alexandra, S. Rahman, S. Masyeni, H. Harapan, S. S. Mamada, T. Bin Emran and F. Nainu, *ADMET DMPK*, 2023, **11**, 331–359.
28 H. Zhao, L. Wu, G. Yan, Y. Chen, M. Zhou, Y. Wu and Y. Li, *Signal Transduction Targeted Ther.*, 2021, **6**, 263.
29 P. C. Agu, C. A. Afiukwa, O. U. Orji, E. M. Ezeh, I. H. Ofoke, C. O. Ogbu, E. I. Ugwuja and P. M. Aja, *Sci. Rep.*, 2023, **13**, 13398.
30 J. E. Fonseca, M. J. Santos, H. Canhão and E. Choy, *Autoimmun. Rev.*, 2009, **8**, 538–542.
31 T. Tanaka, M. Narazaki and T. Kishimoto, *Cold Spring Harbor Perspect. Biol.*, 2014, **6**, a016295.
32 T. D. Gilmore, *Oncogene*, 2006, **25**, 6680–6684.
33 T. Liu, L. Zhang, D. Joo and S.-C. Sun, *Signal Transduction Targeted Ther.*, 2017, **2**, 17023.
34 G. van Loo and M. J. M. Bertrand, *Nat. Rev. Immunol.*, 2023, **23**, 289–303.

35 C. Chen, *Nat. Chem. Biol.*, 2010, **6**, 401–402.
36 A. S. Mendiola and A. E. Cardona, *J. Neural Transm.*, 2018, **125**, 781–795.
37 M. F. Neurath, C. Becker and K. Barbulescu, *Gut*, 1998, **43**, 856–860.
38 Y. Li, X. Wang, J. Ren, X. Lan, J. Li, J. Yi, L. Liu, Y. Han, S. Zhang, D. Li and S. Lu, *BMC Pharmacol. Toxicol.*, 2017, **18**, 5.
39 L. Lima, S. Gaspar, B. S. Rocha, R. Alves and M. G. Almeida, *Clin. Oral Invest.*, 2024, **28**, 521.
40 N. Tuteja, M. Chandra, R. Tuteja and M. K. Misra, *BioMed Res. Int.*, 2004, 498591.
41 S.-H. Baek, T. Park, M.-G. Kang and D. Park, *Molecules*, 2020, **25**, 4089.
42 M. Picard and O. S. Shirihai, *Cell Metab.*, 2022, **34**, 1620–1653.
43 M. C. Martínez and R. Andriantsitohaina, *Antioxid. Redox Signaling*, 2009, **11**, 669–702.
44 K. Sikand, J. Singh, J. S. Ebron and G. C. Shukla, *PLoS One*, 2012, **7**, e47510.
45 E. H. Choy, F. De Benedetti, T. Takeuchi, M. Hashizume, M. R. John and T. Kishimoto, *Nat. Rev. Rheumatol.*, 2020, **16**, 335–345.
46 M. Aliyu, F. T. Zohora, A. U. Anka, K. Ali, S. Maleknia, M. Saffarioun and G. Azizi, *Int. Immunopharmacol.*, 2022, **111**, 109130.
47 C. Popa, M. G. Netea, P. L. van Riel, J. W. van der Meer and A. F. Stalenhoef, *J. Lipid Res.*, 2007, **48**, 751–762.
48 R. Berti, A. J. Williams, J. R. Moffett, S. L. Hale, L. C. Velarde, P. J. Elliott, C. Yao, J. R. Dave and F. C. Tortella, *J. Cereb. Blood Flow Metab.*, 2002, **22**, 1068–1079.
49 S. Mansoor, A. R. Butt, A. Bibi, S. Mushtaq, I. Ullah, F. Alshahrani, A. Khan and A. Mansoor, *PLoS One*, 2023, **18**, e0291332.
50 U. Fiedler and H. G. Augustin, *Trends Immunol.*, 2006, **27**, 552–558.
51 M. K. Jones, H. Wang, B. M. Peskar, E. Levin, R. M. Itani, I. J. Sarfeh and A. S. Tarnawski, *Nat. Med.*, 1999, **5**, 1418–1423.
52 K. M. de la Harpe, P. P. D. Kondiah, Y. E. Choonara, T. Marimuthu, L. C. du Toit and V. Pillay, *Cells*, 2019, **8**, 1209.
53 C. T. Esmon, *Br. J. Haematol.*, 2005, **131**, 417–430.
54 S. Malehmir, M. A. Esmaili, M. Khaksary Mahabady, A. Sobhani-Nasab, A. Atapour, M. R. Ganjali, A. Ghasemi and A. Moradi Hasan-Abad, *Front. Chem.*, 2023, **11**, 1249134.
55 D. G. Remick, D. E. Newcomb, G. L. Bolgos and D. R. Call, *Shock*, 2000, **13**, 110–116.
56 D. R. Brenner, D. Scherer, K. Muir, J. Schildkraut, P. Boffetta, M. R. Spitz, L. Le Marchand, A. T. Chan, E. L. Goode, C. M. Ulrich and R. J. Hung, *Cancer Epidemiol., Biomarkers Prev.*, 2014, **23**, 1729–1751.
57 Y. Fang, Z. Li, L. Yang, W. Li, Y. Wang, Z. Kong, J. Miao, Y. Chen, Y. Bian and L. Zeng, *Cell Commun. Signaling*, 2024, **22**, 276.
58 A. L. Vijayan, N. Vanimaya, S. Ravindran, R. Saikant, S. Lakshmi, R. Kartik and G. M, *J. Intensive Care*, 2017, **5**, 51.
59 I. Siddiqui, L. Jafri, Q. Abbas, A. Raheem and A. U. Haque, *Indian J. Crit. Care Med.*, 2018, **22**, 91–95.
60 P. Liang and F. Yu, *Med. Sci. Monit.*, 2022, **28**, e935966.
61 X. Liu, D. F. Wang, Y. Fang, W. F. Ye, S. Liu and N. Lou, *Leuk. Lymphoma*, 2015, **56**, 85–91.
62 A. Pérez-Pérez, F. Sánchez-Jiménez, T. Vilariño-García and V. Sánchez-Margalet, *Int. J. Mol. Sci.*, 2020, **21**, 5887.
63 A. M. Garofalo, M. Lorente-Ros, G. Goncalvez, D. Carriedo, A. Ballén-Barragán, A. Villar-Fernández, Ó. Peñuelas, R. Herrero, R. Granados-Carreño and J. A. Lorente, *Intensive Care Med. Exp.*, 2019, **7**, 45.
64 K. L. Grinnell, H. Chichger, J. Braza, H. Duong and E. O. Harrington, *Am. J. Respir. Cell Mol. Biol.*, 2012, **46**, 623–632.
65 G. Wang, Z. Hu, Q. Fu, X. Song, Q. Cui, R. Jia, Y. Zou, C. He, L. Li and Z. Yin, *Sci. Rep.*, 2017, **7**, 45006.
66 V. Khanijou, N. Zafari, M. T. Coughlan, R. J. MacIsaac and E. I. Ekinci, *Diabetes Metab. Res. Rev.*, 2022, **38**, e3556.
67 L. Hammerich and F. Tacke, *Nat. Rev. Gastroenterol. Hepatol.*, 2023, **20**, 633–646.
68 Y. Yang, W. Zhong, Y. Zhang, Y. Cheng, H. Lai, H. Yu, N. Feng, Y. Han, R. Huang and Q. Zhai, *J. Inflamm. Res.*, 2022, **15**, 5635–5648.
69 F. Wu, X.-Y. Ding, X.-H. Li, M.-J. Gong, J.-Q. An and S.-L. Huang, *J. Neuroimmunol.*, 2020, **344**, 577264.
70 L. Ma, L. Wang, Y. Qu, X. Wan and K. Hashimoto, *Transl. Psychiatry*, 2023, **13**, 269.
71 M. Resl, M. W. Heinzl, C. Klammer, M. Egger, R. Feldbauer, J. Pohlhammer, B. Dieplinger and M. Clodi, *J. Cardiovasc Transl. Res.*, 2021, **14**, 941–947.
72 A. Bersano, J. Engele and M. K. E. Schäfer, *BMC Neurol.*, 2023, **23**, 227.
73 L. Yang, R. Zhou, Y. Tong, P. Chen, Y. Shen, S. Miao and X. Liu, *Neurobiol. Dis.*, 2020, **140**, 104814.
74 K. L. Swingle, A. G. Hamilton, H. C. Safford, H. C. Geisler, A. S. Thatte, R. Palanki, A. M. Murray, E. L. Han, A. J. Mukalel, X. Han, R. A. Joseph, A. A. Ghalsasi, M.-G. Alameh, D. Weissman and M. J. Mitchell, *Nature*, 2025, **637**, 412–421.
75 D. B. G. Williams and M. Lawton, *J. Org. Chem.*, 2010, **75**, 8351–8354.
76 H. Mori, K. Sutoh and T. Endo, *Macromolecules*, 2005, **38**, 9055–9065.
77 T. Lawrence, *Cold Spring Harbor Perspect. Biol.*, 2009, **1**, a001651.
78 P. Tripathi, P. Tripathi, L. Kashyap and V. Singh, *FEMS Immunol. Med. Microbiol.*, 2007, **51**, 443–452.
79 E. M. Albataineh, S. Abdulrahman, S. S. F. Hussain, H. M. Abd El Kareem and S. S. Mahgoub, *Med. Sci.*, 2021, **25**, 3336–3344.
80 D. G. Remick, D. E. Newcomb, G. L. Bolgos and D. R. Call, *Shock*, 2000, **13**, 110–116.
81 F. Zhao, X. Wang, H. Liu and J. Qian, *J. Funct. Foods*, 2024, **112**, 105983.